Geochemistry, Geophysics, Geosystems

RESEARCH ARTICLE
10.1029/2022GC010771

**Key Points:**

- Large Li isotopic fractionations are observed in rare-metal-rich peraluminous granites
- Fractional crystallization governs Li isotopic behavior and enriches heavier Li isotopes in the highly evolved granites
- Lithium isotopes provide new insights into the granitic magmatic differentiation process and rare-metal mineralization

**Supporting Information:**

Supporting Information may be found in the online version of this article.

**Correspondence to:**

J.-H. Yang and H. Chen,
yangjiehua@vip.gyig.ac.cn;
hengchen@ldeo.columbia.edu

**Citation:**

Yang, J.-H., Chen, H., Zhou, M.-F., Hu, R.-Z., & Williams-Jones, A. E. (2023). Lithium isotope fractionation during intensive felsic magmatic differentiation. *Geochemistry, Geophysics, Geosystems*, *24*, e2022GC010771. https://doi.org/10.1029/2022GC010771

Received 15 NOV 2022
Accepted 1 MAR 2023

**Author Contributions:**

**Conceptualization:** Jie-Hua Yang, Heng Chen, Mei-Fu Zhou
**Data curation:** Jie-Hua Yang, Heng Chen, Rui-Zhong Hu
**Formal analysis:** Jie-Hua Yang, Heng Chen
**Investigation:** Jie-Hua Yang, Heng Chen, Rui-Zhong Hu, Anthony E. Williams-Jones
**Methodology:** Jie-Hua Yang, Heng Chen
**Resources:** Jie-Hua Yang, Heng Chen, Mei-Fu Zhou, Rui-Zhong Hu, Anthony E. Williams-Jones



# Lithium Isotope Fractionation During Intensive Felsic Magmatic Differentiation

**Jie-Hua Yang[1], Heng Chen[2], Mei-Fu Zhou[1], Rui-Zhong Hu[1], and Anthony E. Williams-Jones[3]**

[1]State Key Laboratory of Ore Deposit Geochemistry, Institute of Geochemistry, Chinese Academy of Sciences, Guiyang, China, [2]Lamont-Doherty Earth Observatory, Columbia University, Palisades, NY, USA, [3]Department of Earth and Planetary Sciences, McGill University, Montréal, Québec, Canada

**Abstract** The Xihuashan and Yaogangxian granitic plutons in South China comprise highly evolved multiphase Li-rich granites and host quartz-vein-type tungsten deposits. The $\delta^7$Li values of Phase A (early stage), B (middle stage), and C (late stage) from the Xihuashan pluton are 1.0–1.2‰, 1.1–3.0‰, and 2.4–2.8‰ respectively, increasing through chemical evolution. The granites from the Yaogangxian pluton also display gradually enriched in heavy Li isotopes in a later stage, although systematically lighter than those of the Xihuashan pluton. In both plutons, the $\delta^7$Li shows good correlations with $SiO_2$ and Li concentrations as well as Rb/Sr, Nb/Ta, and Zr/Hf ratios, indicating Li isotopic fractionation most likely caused by magmatic differentiation. In situ analyses show that the minerals of Xihuashan pluton record a continuous elemental spectrum, reflecting the results of progressive magmatic differentiation. The $\delta^7$Li values of quartz, feldspar, mica, and zircon all correlate well with the chemical evolutions of granitic magma, systematically elevated in Phases B and C relative to Phase A. The Li isotope data of the mineral separates further document that the enrichment of $^7$Li in the residual melt was most likely due to the equilibrium fractionation between the mineral and melts. The data are interpreted to reflect that intense magmatic differentiation was responsible for Li isotopic variations coupled with the enrichment in the Li, F, P, and rare metals in the late-phase granites of the Xihuashan pluton. The lithium isotope behavior documented in this study provides new insights into magmatic differentiation and associated rare-metal mineralization.

**Plain Language Summary** In the past, magmatic differentiation was thought not to produce resolvable Li isotopic fractionation based on studies of basaltic rocks. Overall, only sparse studies on Li isotopes of highly evolved granites have been reported, and thus possible isotope fractionation of Li isotopes during differentiation of felsic magma could have been neglected. In this study, we present evidence of Li isotope fractionation during the differentiation of granitic magma. The most evolved (late-stage) rare-metal-rich granites are systematically enriched in heavier Li isotopes. The chemical and isotopic compositions of both bulk rocks and mineral separates (e.g., zircon and mica) indicate that equilibrium fractionation during fractional crystallization governs Li isotopic behavior and enriches heavier Li isotopes in the residual melts. Our quantitative modeling also supports the equilibrium fractionation between minerals and magma as the primary mechanism for the observed Li isotopic variations.

## 1. Introduction

Lithium isotope fractionation has been extensively used to investigate Earth surface processes such as water-rock interaction (Chan et al., 2002) and continental weathering (Pistiner & Henderson, 2003; Rudnick et al., 2004; Vigier et al., 2009; von Strandmann et al., 2017). The large mass difference (~17%) between $^6$Li and $^7$Li and the large scale of fractionation in the upper crust (>80‰ for $\delta^7$Li; Tomascak, 2004; Tomascak et al., 2016) also make Li an isotopic system of considerable interest in tracing subduction zone processes and crustal recycling (Liu et al., 2020; Tang et al., 2014; Tomascak et al., 2016), whereas the high-temperature magmatic differentiation has been thought not to generate resolvable Li isotope fractionation based on studies of terrestrial basaltic rock suites (Schuessler et al., 2009; Tomascak et al., 1999). However, lunar mare basalts exhibit an extensive range of Li isotope compositions ($\delta^7$Li = +3.4‰ to +6.4‰), which correlate with indices of magmatic differentiation (Magna et al., 2006). In addition, large lithium isotopic fractionation has been observed among cogenetic granitic pegmatites (Barnes et al., 2012; Teng et al., 2006). There have also been recent reports of Li isotope fractionation in highly evolved granites (Chen et al., 2018; Li et al., 2018). Because Li is a fluid-mobile and fast-diffusing element, its isotope fractionations in highly evolved granites and pegmatites have been mainly attributed to either

**Supervision:** Rui-Zhong Hu
**Validation:** Jie-Hua Yang, Heng Chen, Mei-Fu Zhou, Rui-Zhong Hu
**Visualization:** Jie-Hua Yang, Heng Chen
**Writing – original draft:** Jie-Hua Yang, Heng Chen, Mei-Fu Zhou
**Writing – review & editing:** Jie-Hua Yang, Heng Chen, Rui-Zhong Hu, Anthony E. Williams-Jones

fluid-melt interaction or diffusion rather than equilibrium fractionation between the minerals and melts (Chen et al., 2018; Holycross et al., 2018; Li et al., 2018; Teng et al., 2006). Overall, there have been limited number of studies on the Li isotopic compositions of highly evolved granitic rocks, and the Li isotope fractionation that may occur during the evolution of granitic magmas has not been properly evaluated. Therefore, if such fractionation does happen, what mechanism controls isotopic fractionation, and what degree of magmatic differentiation is required to generate measurable Li isotope fractionation? Is the Li isotope fractionation during the evolution of granitic magmas recorded in the minerals?

Experimental studies show that the solidification temperatures of granitic bulk compositions are typically 650–700°C (Luth et al., 1964; Piwinskii, 1973). When below the solidus temperature, the crystallized minerals often go through subsolidus re-equilibrium during metamorphism or hydrothermal alteration (London, 2005). Highly evolved S-type rare-metal-rich peraluminous granites have high bulk Li contents, making them ideal candidates for evaluating Li isotope fractionation during progressive differentiation under the intermediate to high-temperature conditions (600–1,000°C, Chappell et al., 2004). The Xihuashan and Yaogangxian granitic plutons in South China comprise highly evolved multiphase and extraordinarily Li-F-rare-metal-rich peraluminous granites. To better understand the Li isotopic fractionation during magmatic differentiation, we measured Li isotopic compositions of bulk rocks, and mineral separates (quartz, feldspar, mica, zircon, and garnet) as well as in situ major and trace elements of minerals (zircon, feldspar, and mica). Combined with bulk-rock chemical data for the different phases of the peraluminous granites from these two plutons, this new data set can help identify possible links between magmatic differentiation and Li isotope fractionation of granites. Utilizing the new mineralogical and isotopic data in conjunction with geochemical modeling, we demonstrate that the elevated $\delta^7$Li values of these rare-metal-mineralized peraluminous granites are most likely the product of intense magmatic differentiation. Thus, the lithium isotopic compositions of these granites could provide new insights into the differentiation of granitic magmas.

## 2. Regional Geology and Samples

Geologically, South China consists of the Cathaysian Block and the Yangtze Block, which are separated by the Jiangshan-Shaoxing Fault (Figure 1a). These two blocks are generally considered to have been welded together during the Neoproterozoic (Zhao & Asimow, 2014). Extensive granitic magmatism and rare-metal mineralization occur in the northeastern part of the Yangtze Block and many parts of the Cathaysia Block during the Mesozoic, particularly in the Nanling Range (Mao et al., 2019) (Figure 1a). The central Nanling Range is located mainly in the Cathaysia Block and contributes more than 50% of the world's tungsten resources (Mao et al., 2019) (Figure 1b). Most deposits are spatially, temporally, and genetically related to highly evolved Middle-Late Jurassic peraluminous granites with high $SiO_2$ contents (>70.0 wt.%) and A/CNK values [molar $Al_2O_3/(K_2O + Na_2O + CaO)$ ratio > 1.1] (Mao et al., 2019). The Xihuashan and Yaogangxian plutons, in the central Nanling Range, host world-class giant quartz vein-type W deposits. Those granite plutons are composed of multiphase, Li-F-rich granites and were emplaced at a shallow crustal level during a short time interval (<4 million years) at about 158 Ma (Li et al., 2011; Yang et al., 2012).

### 2.1. Xihuashan Granitic Pluton

The Xihuashan granitic pluton (25°23′30.01″N, 114°15′29.88″E) intruded Cambrian low-grade metamorphic sedimentary rocks and was exposed over an area of about 20 km$^2$ (Figure 1c). It has been divided into four subunit phases based on detailed geological mapping and petrographic examination (Wu et al., 1987; Yang et al., 2012) (Figure 1c). The first phase, also the least evolved one, is a medium-grained porphyritic granite (Phase A) and occurs mainly in the southern and southwestern parts of the pluton, where it largely surrounds the second phase, a medium-grained two-mica granite (Phase B). The third phase is a fine-grained two-mica granite (Phase C), which occupies much of the northern and northeastern parts of the pluton. The main rare-metal deposits of the Xihuashan pluton are hosted by Phases B and C. An unmineralized fine-grained porphyritic granite (Phase D) is restricted to NW-SE-trending dykes which crosscut phases A to C in the central part of the pluton (Yang et al., 2012). This phase is considered to represent a separate magmatic event (Yang et al., 2012) and is thus not discussed in this paper.

Phase A is composed mainly of quartz (30%–33%), oligoclase (28%–39%), sanidine (15%–25%), and siderophyllite (13%–18%) (Figure S1 in Supporting Information S1). Quartz and oligoclase occur as 1–3 cm long phenocrysts

10.1029/2022GC010771

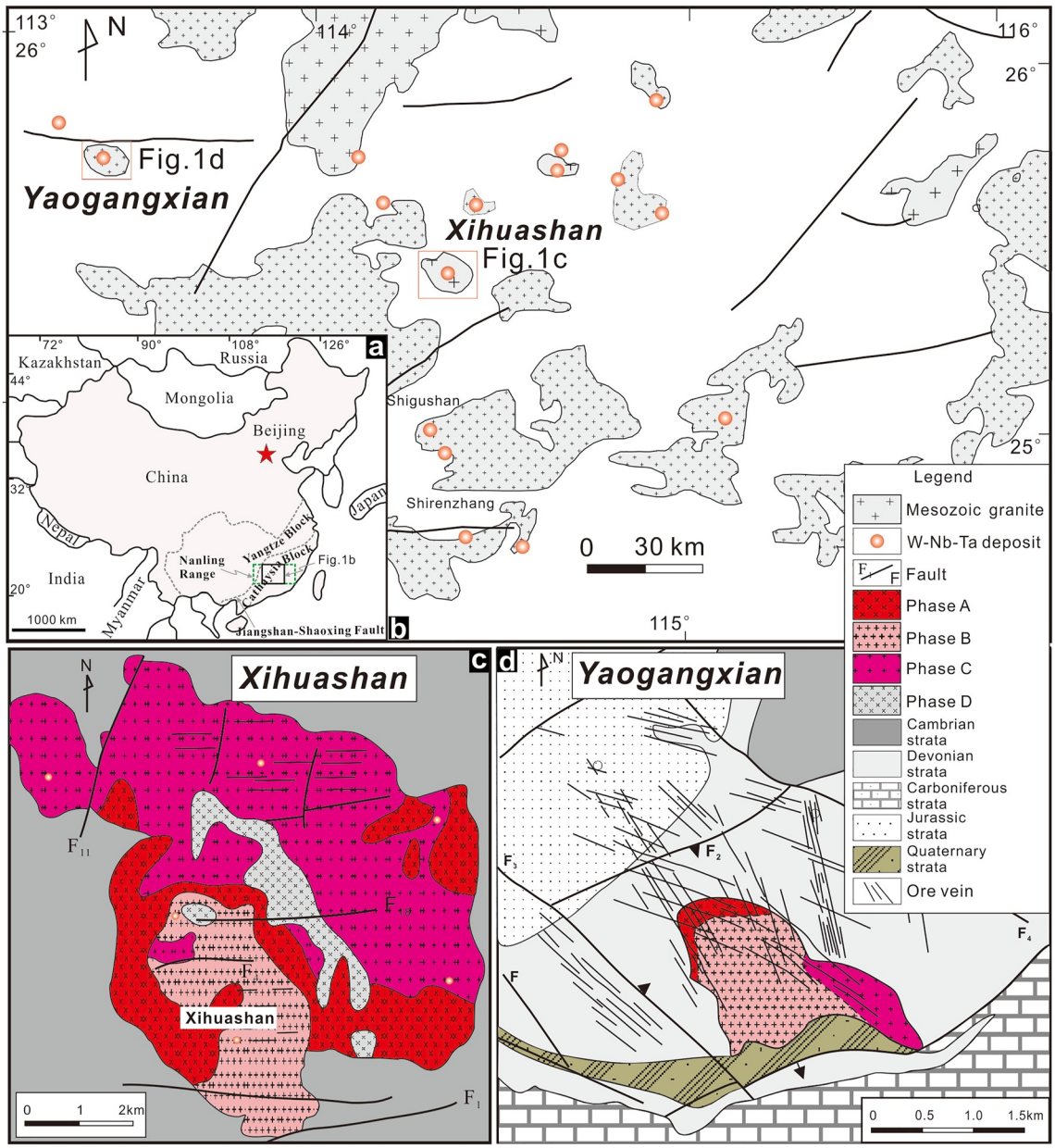


**Figure 1.** Map showing the location of research area (a). A simplified map showing the distribution of important Mesozoic peraluminous granites and major tungsten and niobium-tantalum deposits in the central Nanling Range, South China (b). Geological map of the Xihuashan granitic pluton (c). Geological map of the Yaogangxian granitic pluton and tungsten deposit (d). The map (a) was modified from Mao et al. (2019); (b) was modified from Yang et al. (2018); (c) was modified from Yang et al. (2012); and (d) was modified from Chen (1988).

in a matrix composed mainly of anhedral feldspar grains and fine-grained quartz. Common accessory minerals include monazite, apatite, xenotime, zircon and fluorite. Zircon typically occurs as well-developed prisms (100) with multiple oscillatory growth zones. Phase B consists dominantly of interlocked crystals of quartz (30%–33%), albite (28%–39%), sanidine (16%–26%), and scattered protolithionite (6%–11%) crystals (Figure S1 in Supporting Information S1). Garnet and muscovite are commonly observed, and the garnet is typically enclosed by or included in quartz, feldspar, and mica. Accessory minerals include zircon, fluorite, bastnäsite-(Ce), xenotime-(Y), gadolinite-(Ce), synchysite-(Ce), and thorite. Zircon occurs primarily as euhedral, murky, and porous grains, and in places, shows faint oscillatory growth zones (Figure S2 in Supporting Information S1).

Phase C intrudes into Phase A (Yang et al., 2012) and has a similar mineral assemblage to Phase B but with more garnet and fluorite (Figure S1 in Supporting Information S1). This phase was previously regarded as a marginal

facies of Phase B (Wu et al., 1987; Yang et al., 2012). Granites from Phases B and C contain more quartz, fluorite, and garnet than those from Phase A (Figure S1 in Supporting Information S1). Greisen is widespread along W-bearing quartz veins (see Figure S3 in Supporting Information S1), containing abundant modal zinnwaldite and quartz, and minor muscovite.

### 2.2. Yaogangxian Granitic Pluton

The Yaogangxian granitic pluton (25°39′11.9″N, 113°19′59.75″E) intrudes the Cambrian and Devonian strata, with an outcrop area of 1.2 $km^2$ (Figure 1d). It consists of three subunits, and from the oldest to youngest includes medium-grained porphyritic two-mica granite (Phase A), fine-grained two-mica granite (Phase B), and fine-grained muscovite granite (Phase C) (Dong et al., 2014). These granites mainly consist of K-feldspar, plagioclase, quartz, and muscovite with minor biotite. Granites from Phases B and C contain considerable accessory minerals, such as garnet and fluorite. For a more detailed petrographic description of these granites, readers are referred to Chen (1988) and Dong et al. (2014). W mineralization is spatially, temporally, and genetically associated with the granites (Dong et al., 2014; Mao et al., 2019). The different phases of granites are considered to be co-magmatic and to represent different stages of magmatic evolution (Chen, 1988; Dong et al., 2014).

## 3. Analytical Methods

### 3.1. Bulk-Rock Major and Trace Element Measurement

Major elements of bulk-rock were analyzed with a Pananalytical Axios-advance (Axios PW4400) X-ray fluorescence spectrometer (XRF) at the State Key Laboratory of Ore Deposit Geochemistry, Institute of Geochemistry, Chinese Academy of Sciences (IGCAS). Fused glass discs were used, and the analytical precision, as determined on the Chinese National standards GSR-1(granite) and GSR-3 (granite), is better than 5%. Loss of ignition was obtained using 1 g of powder heated at 1,100°C for 1 hr. Trace element concentrations were determined by the ELAN DRC-e ICP-MS at IGCAS, following procedures described by Qi et al. (2000). The discrepancy between triplicate analyses is less than 5% for all elements. Analyses of standards GSR-1(granite) and GBW07125 (pegmatite) for major elements, and AGV-2 (andesite), AMH-1 (andesite), and GeoPT7 (plagiogneiss) for trace elements are in agreement with the recommended values (Table S1 in Supporting Information S2).

### 3.2. In Situ Chemical Analyses of Minerals

Major element contents of mica, feldspar, and zircon were obtained using an electron microprobe (Shimadzu EPMA-1600) equipped with a wavelength dispersive spectrometer at the IGCAS. An accelerating voltage of 15 kV and a probe current of 10 nA were applied. For mica, well-characterized kaersutite (Na, Ca, Ti, Mn), biotite (K, Mg, Al, Si, Fe), tugtupite (Cl), and apatite (F) were used as standards. For K-feldspar, the standards plagioclase (Na, Al, Si, Ca), pyrope garnet (Mg, Fe), and sanidine (K) were used. For zircon, the standards were pyrope (Si) and $ZrO_2$ (Zr, Hf). Chemical formulae of mica and feldspar were calculated based on 22 and 8 oxygens, respectively.

Trace element concentrations of minerals from the Xihuashan pluton were measured on the exact spots where major elements were previously measured. In situ trace element concentrations were obtained by laser ablation ICP-MS (LA-ICP-MS) using an Agilent 7900 ICP-MS coupled with a GeoLasPro 193 nm ArF excimer laser ablation system at IGCAS. Analytical conditions were as follows: a fluence of 4–5 $J/cm^2$, at a repetition rate of 5–6 Hz, and laser spot of 44 μm for feldspar and mica (ablation duration of 40 s), and 32 μm for zircon. For zircon, Si (determined by EPMA) was selected as the internal standard and the USGS basaltic reference glasses GSE-1G was chosen as the external standard (Liu et al., 2010). Zircon 91500 and NIST 610 (glass) were used to test the analytical reproducibility and accuracy, and the analyzed results are consistent with recommended values (Table S1 in Supporting Information S2). For mica and feldspar, the USGS reference glasses BCR-2G, BHVO-2G, and BIR-1G were analyzed as external standards, and Si (determined by EPMA) was used as the internal standard. Every 5 sample analyses were followed by one analysis of NIST 610 to monitor the time-dependent sensitivity and mass discrimination for the trace element analysis. The accuracy was verified by analyzing SRM 612 (Table S1 in Supporting Information S2). The detailed analytical procedures are similar to Liu et al. (2010). The recommended values of element concentrations for the USGS reference glasses are from the GeoReM database (Jochum et al., 2005).

### 3.3. Li Isotope Compositions of Bulk-Rocks and Minerals

The samples for bulk Li isotopic measurement are the same as those used for major and trace elements (see Section 3.1). The mineral samples from different phases of the Xihuashan pluton were hand-picked under a binocular microscope. For the Li isotope measurement, bulk powder and mineral samples were first digested through a standard two-step protocol (concentrated HF + $HNO_3$ and 6 N HCl). Separation of Li from the matrix was achieved using a chromatography procedure in the clean lab at the University of Sciences and Technology of China (USTC) following the procedure described by Gao and Casey (2012). All separations were monitored with ICP-MS analysis to guarantee both a high Li yield (>99% recovery) and a low Na/Li ratio (<0.01). The total procedural blank determined for the combined sample digestion and column procedure was less than ~0.03 ng for Li, which is negligible compared with the ~200–5,000 ng Li in samples.

The Li isotopic compositions of bulk rocks were analyzed on a Neptune Plus MC-ICP-MS in wet plasma mode using an *X* skimmer cone and a Jet sample cone at USTC. Samples were introduced through a low-flow perfluoroalkylate nebulizer coupled with a quartz spray chamber. For a solution with 100 ppb Li and solution uptake rate of 50 μL/min, the typical intensity of $^7$Li is about 8 V. The analytical results are reported as $\delta^7Li = [(^7Li/^6Li)_{sample}/(^7Li/^6Li)_{standard}-1)] \times 1{,}000$, where the standard is NIST RM-8545 Li-isotope standard. For rock standards, repeat analysis at USTC yielded +8.9 ± 0.2‰ (2SD, $n = 10$) for quality control (QC), −19.3 ± 0.2‰ (2SD, $n = 19$) for USTC-L, and +7.4 ± 0.5‰ (2SD, $n = 9$) for AGV-2, which are within the uncertainty of the previously published results (Penniston-Dorland et al., 2017; Sun et al., 2016). The isotopic analyses of the mineral separates were performed on a Neptune Plus MC-ICP-MS at IGCAS. The analytical procedure is identical to that for bulk-rock Li isotope analyses in the USTC. Replicated measurements of the reference materials QC yielded $\delta^7$Li of 8.6 ± 0.3‰ (2SD, $n = 12$), which within the uncertainty is consistent with previously reported ratios of 8.8 ± 0.2‰ (Sun et al., 2016).

## 4. Results

### 4.1. Bulk-Rock Major and Trace Element

The major and selected trace element compositions of bulk-rock granites from the Xihuashan and Yaogangxian plutons are reported in Table 1 and Table 2, respectively. Granites from the Xihuashan pluton are characterized by higher $SiO_2$ (74.4%–76.6%), $Na_2O$ (3.79%–4.93%), and $K_2O$ (4.16%–4.74%) contents, but lower MgO (0.01%–0.18%), $Fe_2O_3^T$ (0.66%–1.37%), MnO (0.06%–0.10%), $TiO_2$ (0.02%–0.10%), and CaO (0.51%–0.98%) contents. The Li concentrations of granites from the Xihuashan pluton range from 93 to 1,261 ppm. From Phase A to Phases B and C in the Xihuashan pluton, with the increasing of $SiO_2$ content, the $Fe_2O_3^T$, MgO, CaO, $K_2O$, $TiO_2$, $P_2O_5$, Sr, and Ba contents decrease; in contrast, Hf, Nb, Rb, Li, Cs, and W contents increase. Granites from the Yaogangxian pluton display similar variable trends of these elements (Tables 1 and 2). The Zr/Hf and Nb/Ta ratios decrease, and the Rb/Sr ratio increases from Phase A to Phases B and C in both Xihuashan and Yaogangxian plutons (Figures 2 and 3).

### 4.2. In Situ Element Analyses of Minerals

The chemical compositions of mica are reported in Table S2 in Supporting Information S2. A total of 186 analyses were conducted on 11 samples hand-picked from different phases, and all spots were analyzed by both electron microprobe and LA-ICPMS methods. The trioctahedral mica in the samples evolved progressively from siderophyllite in Phase A to protolithionite in Phases B and C (Figure 4a). The Fe (as well as Mn and Ti) contents correlate negatively with the Si contents (Figure 4b). The protolithionites (Phases B and C) are relatively rich in Li, Ta, W, and Sn (Figure S4 in Supporting Information S1), and display a trend of decreasing K/Cs and K/Rb ratios from the siderophyllite of Phase A (Figures 5a–5c).

Fourteen K-feldspar grains from three intrusive phases of the Xihuashan pluton were also analyzed by LA-ICP-MS and EPMA (see Table S3 in Supporting Information S2). All the analyzed grains correspond to sanidine ($Or_{78-100}$) and have high alkali metal contents. The K/Cs and K/Rb ratios of the sanidine correlate negatively with Cs and Rb contents (Figures 5d–5f).

Major and trace elements of zircons are reported in Table S4 in Supporting Information S2. It is common for zircons to encounter mineral inclusions, especially apatite, and monazite, using LA-ICPMS analyses (e.g., Bell et al., 2019). We have employed the light rare earth index LREE-I (Dy/Nd + Dy/Sm) < 50 to filter the zircon suites that were

**Table 1**
*Major Elemental Compositions (in wt.%) for Granites From the Xihuashan and Yaogangxian Plutons*

| Samples | Unit | $SiO_2$ | $Al_2O_3$ | $Fe_2O_3T$ | MgO | CaO | $Na_2O$ | $K_2O$ | MnO | $TiO_2$ | $P_2O_5$ | L.O.I | Total |
|---|---|---|---|---|---|---|---|---|---|---|---|---|---|
| Xihuashan pluton | | | | | | | | | | | | | |
| XHS-5 | Phase A | 75.6 | 13.5 | 1.32 | 0.16 | 0.98 | 4.07 | 4.43 | 0.07 | 0.09 | 0.03 | 0.57 | 100.8 |
| XHS-6 | | 75.1 | 12.8 | 1.37 | 0.18 | 0.89 | 5.23 | 4.21 | 0.08 | 0.10 | 0.03 | 0.60 | 100.6 |
| XHS-18 | | 74.4 | 13.1 | 1.12 | 0.13 | 0.99 | 3.80 | 4.74 | 0.07 | 0.09 | 0.02 | 0.49 | 98.9 |
| XHS-21 | | 75.4 | 13.0 | 0.93 | 0.08 | 0.89 | 3.79 | 4.65 | 0.06 | 0.07 | 0.01 | 0.73 | 99.6 |
| XHS-9 | Phase B | 75.6 | 13.0 | 0.80 | 0.03 | 0.59 | 4.24 | 4.24 | 0.09 | 0.02 | <0.01 | 0.96 | 99.6 |
| XHS-12 | | 76.1 | 13.5 | 0.66 | 0.04 | 0.57 | 4.93 | 4.23 | 0.10 | 0.02 | <0.01 | 0.53 | 100.7 |
| XHS-16 | | 75.4 | 13.0 | 0.81 | 0.01 | 0.57 | 4.19 | 4.47 | 0.07 | 0.02 | <0.01 | 0.85 | 99.4 |
| XHS-20 | | 76.1 | 12.9 | 0.69 | 0.03 | 0.62 | 4.65 | 4.16 | 0.08 | 0.02 | <0.01 | 0.63 | 99.9 |
| XHS-7 | Phase C | 75.7 | 13.1 | 0.92 | 0.02 | 0.60 | 4.59 | 4.25 | 0.07 | 0.02 | <0.01 | 0.44 | 99.7 |
| XHS-10 | | 76.4 | 13.1 | 0.83 | 0.03 | 0.51 | 4.60 | 4.23 | 0.15 | 0.02 | <0.01 | 0.71 | 100.6 |
| X-3 | Greisen | 75.7 | 12.9 | 3.10 | 0.05 | 0.75 | 1.73 | 3.88 | 0.19 | 0.01 | <0.01 | 1.62 | 99.9 |
| X-8 | | 61.9 | 21.1 | 3.55 | 0.14 | 0.76 | 3.41 | 5.28 | 0.26 | 0.06 | <0.01 | 2.60 | 99.1 |
| X-14 | | 72.4 | 12.8 | 4.89 | 0.17 | 1.55 | 0.09 | 4.65 | 0.27 | 0.10 | 0.01 | 2.35 | 99.3 |
| X-16 | | 77.1 | 12.6 | 2.66 | 0.17 | 1.06 | 0.09 | 4.17 | 0.15 | 0.07 | <0.01 | 2.16 | 100.2 |
| XHS-4 | Granite | 74.9 | 13.2 | 1.72 | 0.32 | 1.53 | 3.00 | 4.13 | 0.06 | 0.15 | 0.04 | 0.55 | 99.6 |
| XHS-9 | | 74.7 | 13.8 | 1.00 | 0.05 | 0.62 | 4.20 | 4.58 | 0.08 | 0.02 | <0.01 | 0.61 | 99.7 |
| XHS-11 | | 75.3 | 12.8 | 1.53 | 0.26 | 1.19 | 3.09 | 4.65 | 0.07 | 0.13 | 0.03 | 0.59 | 99.6 |
| XHS-6 | | 82.5 | 9.7 | 0.44 | 0.02 | 0.21 | 2.81 | 3.55 | 0.01 | <0.01 | 0.01 | 0.32 | 99.6 |
| XHS-7 | | 75.6 | 13.4 | 0.98 | 0.04 | 0.51 | 4.15 | 4.24 | 0.14 | 0.01 | <0.01 | 0.69 | 99.8 |
| XHS-1 | Greisen | 81.4 | 9.0 | 3.28 | 0.09 | 0.65 | 0.38 | 2.99 | 0.15 | 0.03 | <0.01 | 1.45 | 99.4 |
| XHS-12 | | 79.8 | 9.7 | 3.36 | 0.06 | 0.92 | 0.08 | 3.3 | 0.19 | 0.02 | <0.01 | 1.93 | 99.4 |
| Yaogangxian pluton | | | | | | | | | | | | | |
| ZK501-12 | Phase A | 74.9 | 13.3 | 0.95 | 0.16 | 0.85 | 4.34 | 5.11 | 0.13 | 0.05 | 0.01 | 0.65 | 100.5 |
| YGX-13 | | 76.1 | 13.1 | 0.78 | 0.05 | 0.69 | 3.91 | 4.46 | 0.08 | 0.03 | 0.01 | 0.82 | 100.0 |
| YGX-44 | | 74.8 | 13.2 | 0.89 | 0.04 | 0.60 | 3.72 | 4.83 | 0.14 | 0.03 | 0.01 | 0.60 | 98.9 |
| YGX-11 | Phase B | 76.3 | 12.9 | 0.73 | 0.03 | 0.61 | 3.73 | 4.47 | 0.13 | 0.02 | 0.01 | 0.57 | 99.5 |
| YGX-14 | | 75.7 | 13.0 | 0.81 | 0.03 | 0.63 | 4.01 | 4.41 | 0.12 | 0.02 | 0.01 | 0.88 | 99.6 |
| YGX-35 | | 76.9 | 13.0 | 0.66 | 0.06 | 0.38 | 3.97 | 4.06 | 0.12 | 0.02 | 0.01 | 0.54 | 99.7 |
| ZK501-20 | Phase C | 77.8 | 12.4 | 0.65 | 0.15 | 0.71 | 4.48 | 4.49 | 0.08 | 0.04 | 0.01 | 0.84 | 101.7 |
| ZK501-17 | | 77.5 | 13.2 | 0.54 | 0.13 | 0.41 | 5.17 | 3.84 | 0.06 | 0.01 | <0.01 | 0.98 | 101.8 |
| YGX-41 | | 80.5 | 11.0 | 0.27 | 0.10 | 0.37 | 3.20 | 3.58 | 0.05 | 0.01 | 0.01 | 0.56 | 99.7 |
| YGX-37 | Greisen | 75.2 | 13.2 | 0.96 | 0.05 | 0.71 | 3.60 | 4.49 | 0.14 | 0.04 | 0.01 | 1.84 | 100.2 |
| YGX-16 | | 81.1 | 9.9 | 1.36 | 0.13 | 0.82 | 0.08 | 3.32 | 0.43 | 0.03 | 0.02 | 1.18 | 98.4 |
| ZK501-23 | | 75.8 | 13.1 | 0.67 | 0.19 | 0.47 | 5.38 | 4.31 | 0.14 | 0.01 | 0.01 | 1.96 | 102.0 |

*Note*. L.O.I is loss on ignition.

contaminated by mineral inclusion or aqueous alteration based on the methods described in Bell et al. (2019). The remaining analyses had LREE-I > 50 (Table S4 in Supporting Information S2). The chondrite-normalized rare earth element (REE) profiles of zircons from the three phases granites of the Xihuashan pluton are broadly similar to positive Ce anomalies, negative Eu anomalies, and strong enrichment of the heavy rare earth element (Figure S5 in Supporting Information S1). The backscattered electron images show that zircons in Phase A from the Xihuashan pluton do not exhibit compositional zoning (see Figure S2 in Supporting Information S1), in contrast to those from other phases, with the outer inclusion-free rims of these crystals commonly enriched in Hf. In Phases B and C, the

**Table 2**
*Li Isotopic and Selected Trace Elemental Compositions for Granites From the Xihuashan and Yaogangxian Plutons*

| Samples | Unit | Li | $\delta^7$Li (‰) | 2SD | Zr | Hf | Nb | Ta | Rb | Sr | Cs | Ba | W | Zr/Hf | Nb/Ta | Rb/Sr | F[a] | 2SD | |
|---|---|---|---|---|---|---|---|---|---|---|---|---|---|---|---|---|---|---|---|
| Xihuashan pluton | | | | | | | | ppm | | | | | | | | | | | |
| XHS-5 | Phase A | 105 | 1.05 | 0.08 | 102.0 | 5.35 | 20.2 | 7.6 | 628 | 41.0 | 32.1 | 97.2 | 4.2 | 19.0 | 2.67 | 15.3 | 0.57 | 0.15 | This study |
| XHS-6 | | 93 | 0.95 | 0.28 | 104.0 | 4.84 | 23.1 | 9.5 | 623 | 39.4 | 26.1 | 92.5 | 4.3 | 21.4 | 2.43 | 15.8 | 0.50 | 0.14 | |
| XHS-18 | | 98 | 1.25 | 0.30 | 87.3 | 4.27 | 16.6 | 5.7 | 561 | 48.1 | 19.0 | 148.0 | 12.6 | 20.4 | 2.94 | 11.7 | 0.65 | 0.15 | |
| XHS-21 | | 118 | 1.24 | 0.30 | 78.1 | 4.48 | 23.9 | 8.7 | 655 | 34.6 | 23.3 | 107.0 | 14.3 | 17.4 | 2.73 | 18.9 | 0.66 | 0.14 | |
| XHS-9 | Phase B | 146 | 1.28 | 0.30 | 59.4 | 5.36 | 40.8 | 30.3 | 943 | 7.94 | 28.6 | 63.4 | 24.0 | 11.1 | 1.35 | 119 | 0.92 | 0.03 | |
| XHS-12 | | 170 | 1.58 | 0.30 | 74.7 | 6.03 | 30.5 | 14.1 | 994 | 9.75 | 41.1 | 10.6 | 51.9 | 12.4 | 2.17 | 102 | 0.93 | 0.01 | |
| XHS-16 | | 151 | 2.02 | 0.12 | 75.9 | 6.48 | 27.6 | 16.8 | 1031 | 8.20 | 44.1 | 11.2 | 35.0 | 11.7 | 1.64 | 126 | 0.93 | 0.03 | |
| XHS-20 | | 124 | 3.02 | 0.17 | 63.0 | 5.39 | 30.4 | 19.0 | 991 | 6.88 | 38.8 | 11.2 | 44.1 | 11.7 | 1.60 | 144 | 0.94 | 0.02 | |
| XHS-7 | Phase C | 199 | 2.45 | 0.30 | 55.9 | 5.07 | 26.2 | 20.2 | 983 | 5.10 | 48.5 | 9.0 | 59.5 | 11.0 | 1.30 | 193 | 0.93 | 0.01 | |
| XHS-10 | | 141 | 2.76 | 0.30 | 65.9 | 5.72 | 34.6 | 21.6 | 971 | 8.41 | 73.6 | 5.7 | 65.6 | 11.5 | 1.60 | 115 | 0.90 | 0.01 | |
| X-3 | Greisen | 1093 | −3.92 | 0.30 | 61.7 | 4.59 | 13.2 | 5.3 | 980 | 4.33 | 54.5 | 13.7 | 31.5 | 13.4 | 2.49 | 226 | – | – | |
| X-8 | | 870 | −4.18 | 0.30 | 49.5 | 4.40 | 32.5 | 19.6 | 1540 | 6.90 | 101.0 | 10.9 | 32.6 | 11.3 | 1.65 | 223 | – | – | |
| X-14 | | 1261 | −2.72 | 0.30 | 57.0 | 4.45 | 11.1 | 4.9 | 1480 | 3.22 | 84.4 | 77.0 | 42.9 | 12.7 | 2.26 | 460 | – | – | |
| X-16 | | 769 | −1.67 | 0.30 | 76.9 | 5.23 | 13.2 | 7.3 | 1070 | 2.78 | 70.6 | 51.7 | 32.4 | 14.8 | 1.79 | 385 | – | – | |
| XHS-4 | Granite | 166 | 0.56 | 0.04 | 113.0 | 4.30 | 13.3 | 3.9 | 312 | 90.6 | 24.0 | 212.0 | 54.5 | 26.2 | 3.44 | 3.40 | – | – | Li, 2015 |
| XHS-9 | | 90 | 0.45 | 0.05 | 59.5 | 4.59 | 27.2 | 14.4 | 721 | 7.79 | 29.9 | 9.2 | 5.2 | 13.0 | 1.89 | 92.4 | – | – | |
| XHS-11 | | 209 | 0.66 | 0.04 | 85.5 | 3.71 | 11.9 | 3.9 | 472 | 66.1 | 30.5 | 142.0 | 653.0 | 23.0 | 3.05 | 7.14 | – | – | |
| XHS-6 | | 140 | 2.03 | 0.25 | 74.2 | 7.19 | 25.1 | 21.4 | 854 | 4.23 | 63.7 | 3.3 | 4.8 | 10.3 | 1.17 | 202 | – | – | |
| XHS-7 | | 38 | 4.25 | 0.48 | 42.8 | 4.71 | 17.6 | 27.2 | 503 | 5.06 | 11.1 | 3.9 | 11.3 | 9.1 | 0.65 | 99.4 | – | – | |
| XHS-1 | Greisen | 986 | −6.37 | 0.04 | 49.7 | 4.24 | 23.3 | 9.9 | 1010 | 1.76 | 73.5 | 3.7 | 15.8 | 11.7 | 2.35 | 574 | – | – | |
| XHS-12 | | 441 | −5.86 | 0.03 | 50.8 | 4.01 | 13.8 | 5.4 | 1020 | 1.31 | 51.7 | 7.9 | 17.6 | 12.7 | 2.55 | 779 | – | – | |

10.1029/2022GC010771

**Table 2**
*Continued*

| Samples | Unit | Li | $\delta^7$Li (‰) | 2SD | Zr | Hf | Nb | Ta | Rb | Sr | Cs | Ba | W | Zr/Hf | Nb/Ta | Rb/Sr | F[a] | 2SD | |
|---|---|---|---|---|---|---|---|---|---|---|---|---|---|---|---|---|---|---|---|
| Yaogangxian pluton | | | | | | | | | | | | | | | | | | | |
| ZK501-12 | Phase A | 197 | −1.86 | 0.30 | 82.4 | 4.85 | 31.5 | 20.3 | 968 | 18.3 | 16.2 | 21.3 | 32.2 | 17.0 | 1.55 | 52.9 | – | – | This study |
| YGX-13 | | 149 | −1.96 | 0.30 | 68.1 | 4.92 | 40.5 | 32.1 | 298 | 9.93 | 79.1 | 26.8 | 11.6 | 13.8 | 1.26 | 30.0 | – | – | |
| YGX-44 | | 230 | −2.07 | 0.30 | 70.1 | 5.10 | 33.4 | 29.0 | 348 | 7.58 | 36.5 | 15.2 | 36.5 | 13.7 | 1.15 | 45.9 | – | – | |
| YGX-11 | Phase B | 286 | −0.63 | 0.30 | 54.5 | 4.78 | 30.4 | 32.1 | 348 | 5.79 | 61.0 | 12.9 | 94.7 | 11.4 | 0.95 | 60.0 | – | – | |
| YGX-14 | | 257 | −1.29 | 0.30 | 51.6 | 4.02 | 38.5 | 34.0 | 280 | 4.12 | 36.2 | 16.4 | 50.7 | 12.8 | 1.13 | 68.0 | – | – | |
| YGX-35 | | 301 | −0.04 | 0.30 | 64.0 | 5.86 | 35.4 | 41.6 | 331 | 3.35 | 29.6 | 11.3 | 61.0 | 10.9 | 0.85 | 99.0 | – | – | |
| ZK501-20 | Phase C | 296 | 0.23 | 0.30 | 66.9 | 7.43 | 32.1 | 62.4 | 778 | 5.08 | 34.9 | 14.0 | 101.0 | 9.0 | 0.52 | 153 | – | – | |
| ZK501-17 | | 575 | −0.38 | 0.30 | 104.0 | 10.60 | 48.6 | 56.4 | 1200 | 18.1 | 29.4 | 12.9 | 162.0 | 9.8 | 0.86 | 122 | – | – | |
| YGX-41 | | 374 | 0.05 | 0.30 | 56.3 | 6.91 | 31.2 | 95.2 | 400 | 3.31 | 43.0 | 13.7 | 108.0 | 8.1 | 0.33 | 121 | – | – | |
| YGX-37 | Greisen | 193 | −4.33 | 0.30 | 67.8 | 9.69 | 38.9 | 64.8 | 298 | 9.97 | 27.4 | 36.9 | 55.5 | 7.0 | 0.59 | 30.0 | – | – | |
| YGX-16 | | 228 | −3.26 | 0.30 | 36.8 | 5.75 | 21.9 | 72.6 | 276 | 7.42 | 35.2 | 43.3 | 118.0 | 6.4 | 0.30 | 37.0 | – | – | |
| ZK501-23 | | 109 | −3.22 | 0.30 | 40.3 | 4.46 | 23.5 | 30.4 | 362 | 6.35 | 38.3 | 9.3 | 19.7 | 9.0 | 0.77 | 57.0 | – | – | |

[a]The degrees of differentiation (F) for granite samples are calculated using Rb contents of mica and U contents of zircon.

zircons have higher REE, U, Th, P, and Hf contents than in Phase A (Table S4 in Supporting Information S2). The hafnium contents of the zircons are negatively correlated with the Zr/Hf ratios (Figure S6 in Supporting Information S1), and the U content correlates positively with the Th and REE contents (Figure S6 in Supporting Information S1). The incorporation of P in zircon is accompanied by higher REE contents (Figure S5 in Supporting Information S1), similar to the behavior noted by Hanchar et al. (2001).

### 4.3. Li Isotope Compositions of Bulk-Rock and Minerals

The Li isotopic compositions of bulk granites are listed in Table 2. On average, granites from Phases B and C in the Xihuashan pluton have higher $\delta^7$Li values (+1.1 to +3.0‰) than Phase A (+1.0 to +1.2‰) (Figure 2). In contrast, the greisens have $\delta^7$Li values as low as −4.3‰. Granites from the Yaogangxian pluton have a similar Li isotopic variation trend as the Xihuashan pluton, with the $\delta^7$Li increasing from Phase A (−2.1 to −1.9‰) to Phase B (−1.3 to 0.0‰), and Phase C (−0.4 to 0.2‰) (Figure 3). Greisen samples from the Yaogangxian pluton also exhibit distinctively lighter Li isotopic composition ($\delta^7$Li: −4.3 to −3.2‰). For both plutons, there is a marked correlation between $\delta^7$Li value and $SiO_2$ content and Zr/Hf, Nb/Ta, and Rb/Sr ratios (Figures 2 and 3).

The Li concentrations and isotopic compositions of mineral separates of Xihuashan pluton are reported in Table 3. Generally, the $\delta^7$Li values of the minerals in Phases B and C are higher than those of the corresponding minerals in Phase A. The $\delta^7$Li values of zircon, mica, and feldspar all showed good correlations with the chemical compositions of these minerals. Garnet and mica, which contain 486–581 ppm and 2,897–6,641 ppm Li, respectively, are the major Li-bearing minerals (Figure 6a). Garnets from Phases B and C have $\delta^7$Li values of −2.2 to −3.6‰. The $\delta^7$Li values of the trioctahedral micas ranged from −1.9 to 0.8‰, higher than the mica from the greisen (−3.0‰). Quartz has low Li concentrations (11.1–31.4 ppm) and the highest $\delta^7$Li values (13.7–18.3‰) relative to the mica. The plagioclase and K-feldspar have overall low Li concentrations (16.0–41.2 ppm) and highly variable $\delta^7$Li values (−4.0 to 2.2‰). Zircon has a low Li content (24.0–49.4 ppm) and $\delta^7$Li values between −3.3 and 1.6‰.

## 5. Discussion

Granites from the Xihuashan and Yaogangxian plutons show evidence of Li isotope fractionation through magmatic differentiation, as the more evolved phases are enriched in heavier Li isotopes. The $\delta^7$Li values of quartz, plagioclase, K-feldspar, mica, and zircon from Phases B and C of the Xihuashan pluton are systematically higher than those from Phase A, consistent with the Li isotope fractionation trend of the bulk-rocks. Until now, very few studies have quantitatively evaluated the detailed role of magmatic differentiation in Li isotope fractionation. Indeed, Li isotopic variations in granites can theoretically be caused by inherited heterogeneous sources, assimilation of country rocks, fluid exsolution, and magma degassing.

Previous studies proposed that heterogeneous crustal sources are likely the reason for the Li isotope variations observed in felsic magmas (Deveaud et al., 2015; Magna et al., 2016). However, the different phases of granites in the Xihuashan pluton have overlapping U-Pb isotopic ages (156.9–159.5 Ma), zircon Hf-O isotope [$\varepsilon_{Hf}$(t) values of −11.4 to −10.4, $\delta^{18}$O values of 8.6–10.4‰], and initial Nd isotope compositions [$\varepsilon_{Nd}$(t) values of −11.3 to

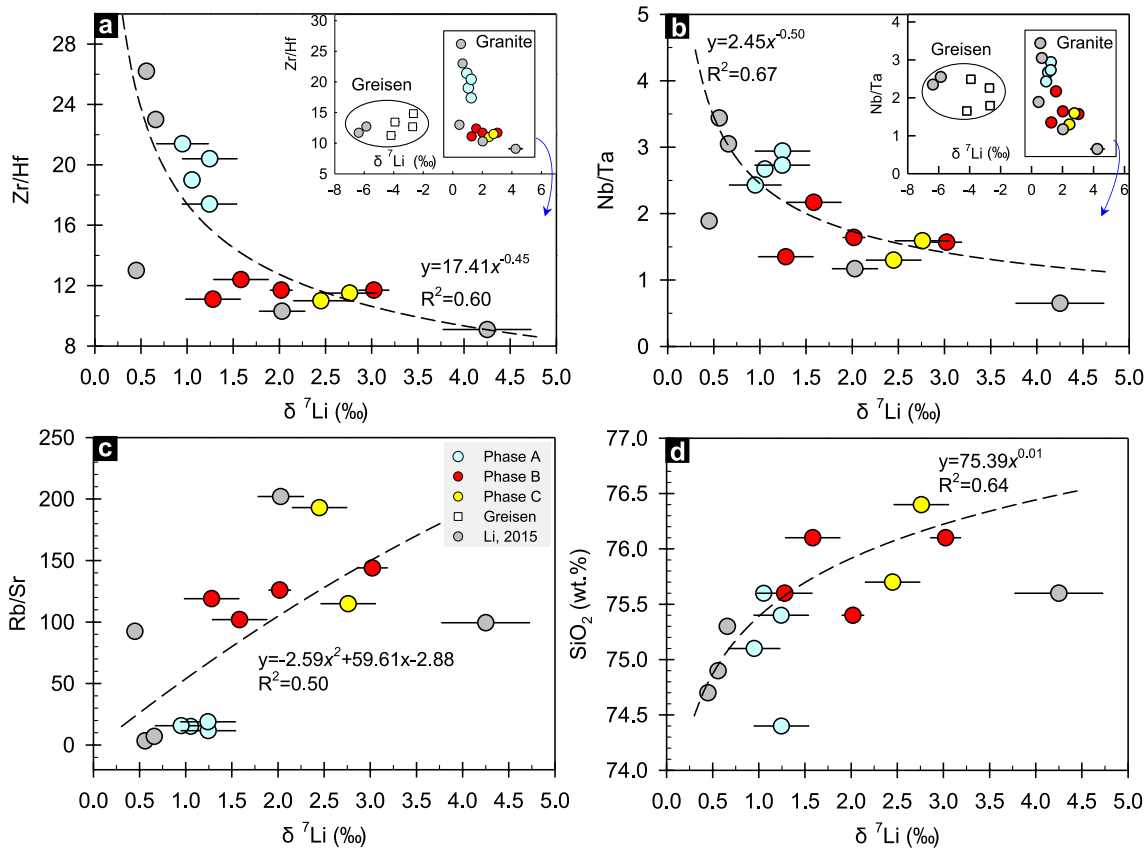


**Figure 2.** Plots showing the relationship between $\delta^7$Li and chemical compositions for granites from the Xihuashan granitic pluton. Two greisen data are from Li (2015).

−10.4] (Guo et al., 2012; Yang et al., 2012), which point to a common origin for different phases. Similarly, granites from the three intrusive phases in the Yaogangxian pluton crystallized from magmas with overlapping zircon U-Pb ages (155.4–158.4 Ma) and bulk-rock Sr-Nd isotope compositions [initial $^{87}$Sr/$^{86}$Sr ratio of 0.7159–0.7318, $\varepsilon_{Nd}$(t) values of −11.3 to −8.4] (Dong et al., 2014; Li et al., 2011). The three different phases in the Yaogangxian pluton are also derived from the same origin. Moreover, since the granites are enriched in Li by a factor as high as 1,000 relative to surrounding metasedimentary rocks (Chen et al., 2018), it requires contamination from very large volumes of metasedimentary rocks to potentially change the Li isotopes in granites during emplacement, which is very unlikely for those two plutons (Magna et al., 2016).

Based on chemical and isotopic characteristics, the granites in the Xihuashan and Yaogangxian plutons are inferred to be the products of partial melting of metapelites (Dong et al., 2014; Yang et al., 2018). Indeed, metapelites are known to have high Li contents and a modest variability in $\delta^7$Li (Teng et al., 2007). Incongruent melting of such metapelites may potentially produce Li isotope variation in the melt (Sun et al., 2016). However, a previous study showed that the Neoproterozoic S-type granites in South China have Li isotope compositions similar to those of Shuangqiaoshan Group metapelites (Chen et al., 2018). There is no noticeable Li isotope change in residual granulite after the metamorphism/anatexis of the pelitic rock despite significant Li loss (~50%) (Qiu et al., 2011; Teng et al., 2007). Therefore, the isotopic fractionation during the partial melting of pelitic rock is rather limited. Moreover, the three phases of the Yaogangxian and Xihuashan plutons evolved from their common parental magma. Thus, Li isotope fractionation during incongruent melting of metapelites can be negligible.

Experimental studies have shown the existence of measurable Li isotopic fractionation between minerals and coexisting fluids at 500–900°C, as a hydrothermal alteration preferentially removes $^7$Li from solids (Wunder et al., 2006, 2011). Experiments have confirmed that the Li isotope fractionation factor [$\alpha_{fluid/melt} = (^7Li/^6Li)_{fluid}/(^7Li/^6Li)_{melt}$] ranges from 1.0024 to 1.0043 at temperatures of 400–670 °C, and the Li isotopic fractionation factor increases with decreasing temperature (Marschall et al., 2007; Wunder et al., 2006, 2007). Teng et al. (2006) suggested an $\alpha_{fluid/melt}$ of ~1.004 as

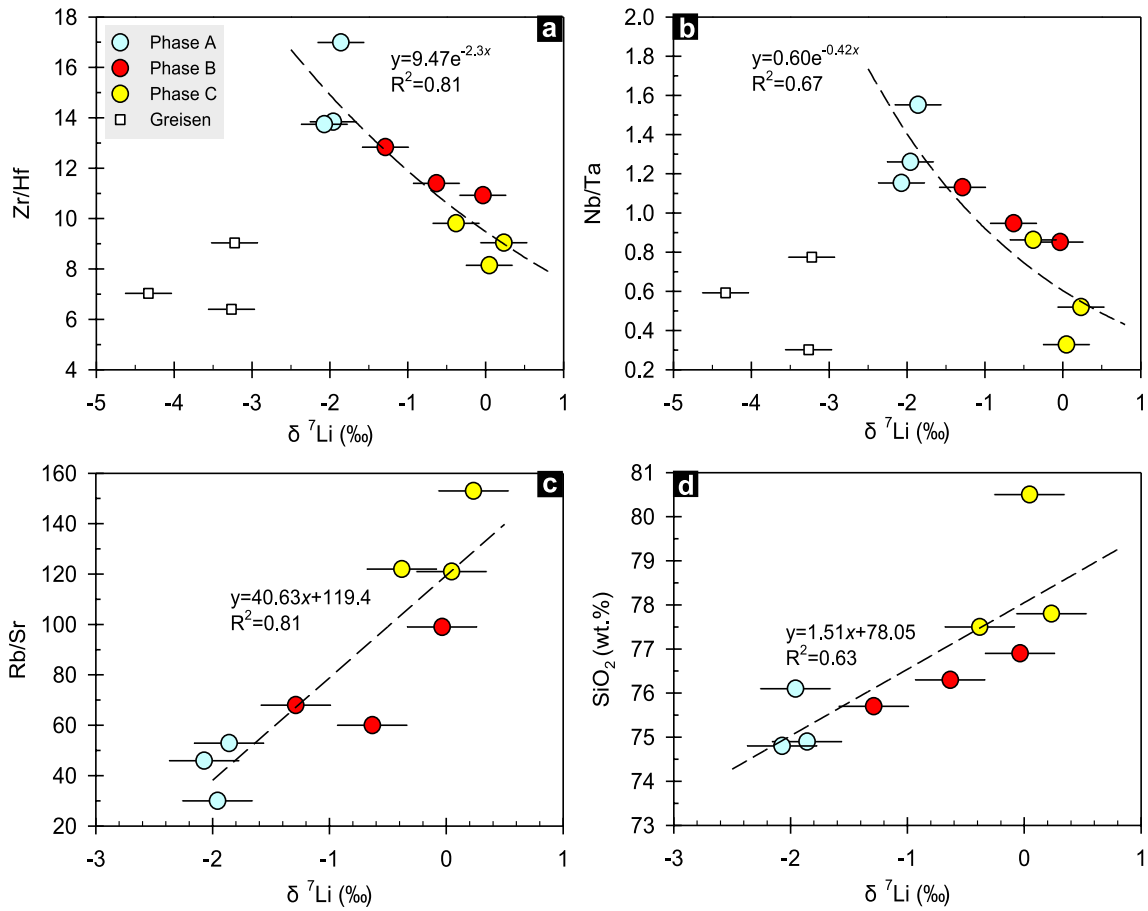


**Figure 3.** Plots showing the relationship between $\delta^7$Li and chemical compositions for granites from the Yaogangxian granitic pluton.

the upper limit value. Although the experimentally determined values of the Li isotope fractionation factor between vapor and melt ($\alpha_{vapor/melt} = (^7Li/^6Li)_{vapor}/(^7Li/^6Li)_{melt}$) are currently not available, a study by Vlastélic et al. (2011) reported that after magma degassing, lava (pumice) from Reunion Island have measurably lighter Li isotopes, which is due to preferred partitioning of the heavy isotope into a coexisting vapor during equilibrium fractionation. The preferential loss of heavy Li isotopes indicates that during magma degassing, Li isotopes are mainly controlled by chemical rather than kinetic effects. The $\alpha_{vapor/melt}$ was constrained as high as 1.010 (Vlastélic et al., 2011).

We employ a simple Rayleigh model to evaluate the Li isotope fractionation during fluid exsolution and magma degassing processes. As mentioned above, the metapelite can be considered the source of rare-metal granites in South China. We assume that the starting magma (the same as metapelite in the upper continental crust from South China) has an initial composition of $\delta^7$Li value of 0‰ and Li content of 24 ppm (Chi & Yan, 2007; Rudnick & Gao, 2003; Teng et al., 2004). The Rayleigh model indicates that fluid exsolution or magma degassing would significantly fractionate the Li isotopic compositions of granitic melt and lead to a lighter $\delta^7$Li toward the more evolved granitic magma (Figure S7 in Supporting Information S1). A previous study found that the mica in the Xihuashan exhibit compositional zoning, indicating extensive fluid-rock interaction (Li et al., 2018). However, the $\delta^7$Li values of the late-stage granites are elevated, obviously opposite to the results of fluid exsolution or magma degassing processes. In contrast, the greisens in the Xihuashan and Yaogangxian plutons have much higher Li concentrations and lower $\delta^7$Li values than those of granites. The greisens consist essentially of quartz and mica, which has a Li concentration of thousand ppm and dominates the Li budget (Table 3). The low $\delta^7$Li in greisen is consistent with the results of either evolved magma with fluid exsolution or subsodius fluid-mineral interaction. During the interaction with fluid or loss of volatile, heavier Li isotopes partition more readily into fluid or vapor phases, leaving the residue greisens enriched lighter Li isotopes. Indeed, subsolidus fluid-rock interaction is widespread in the mining area of the Xihuashan and Yaogangxian plutons, and the Li is likely leached into the fluid during fluid-mineral interactions (Li et al., 2018).

As discussed above, the Li isotope variations between different phases of Xihuashan and Yaogangxian plutons are unlikely controlled by the heterogeneity of their sources, country rock contamination, incongruent melting, fluid exsolution, or magma degassing. Thus, we consider that the primary control on the elevated $^{7}Li/^{6}Li$ ratios in the more evolved granites of the Xihuashan and Yaogangxian plutons is exerted by fractional crystallization.

### 5.1. Magmatic Differentiation Records

Trace-element ratios, notably Rb/Sr, Zr/Hf, and Nb/Ta, provide robust indicators of the felsic magmatic differentiation due to the crystallization of feldspar, mica, and accessory minerals such as monazite, allanite, and zircon (Linnen & Keppler, 2002; Stepanov et al., 2014). The Rb/Sr ratios are clearly elevated, and the Nb/Ta and Zr/Hf ratios are down in the late-stage granites from both Xihuashan and Yaogangxian plutons (Figures 2 and 3), indicating continuous fractional crystallization (Linnen & Keppler, 2002).

Zircon, trioctahedral mica, and K-feldspar from all three phases of granites in the Xihuashan pluton display a continuous compositional spectrum (Figures 4 and 5; Figure S6 in Supporting Information S1). In the Xihuashan pluton, Al and Li are positively correlated with Si. In contrast, Fe, Mn, and Ti are negatively associated with Si in trioctahedral micas (Figure 4), consistent with magmatic differentiation (Hulsbosch et al., 2014). The continuous chemical evolution can also be confirmed by the exponential decrease of K/Rb and K/Cs ratios with increasing Rb and Cs contents in trioctahedral mica (Figures 5b and 5c). These trends for alkali metals in mica are most evident in highly evolved granites and were most generated by fractional crystallization (Hulsbosch et al., 2014, 2016). Like the trioctahedral mica, the K/Rb and K/Cs ratios of K-feldspar decrease exponentially with increasing Rb and Cs contents from Phase A to Phases B and C, which corresponds directly to the differences in the degree of magmatic differentiation (Figures 5e and 5f). Phase B and C zircons have higher U, Th, Hf, P, and REE contents than those from Phase A (Figures S5 and S6 in Supporting Information S1). The U contents were positively correlated with the Th, Eu/Eu*, and REE contents (Figure S6 in Supporting Information S1). The Zr/Hf ratios

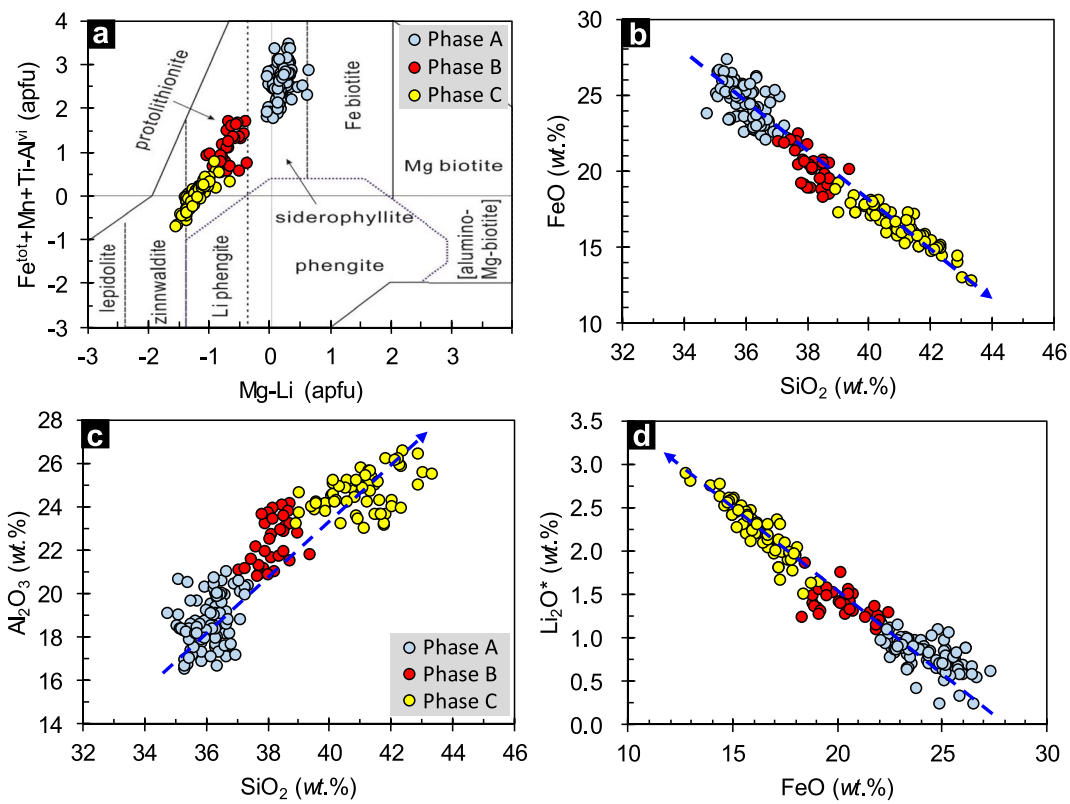


**Figure 4.** A chemical discrimination diagram indicating the types of mica present in the Xihuashan pluton (a). Binary plots showing the chemical composition of mica in the different intrusive phases of the Xihuashan pluton (b–d). The empirical diagram for discriminating the type of mica is after Tischendorf et al. (1997).

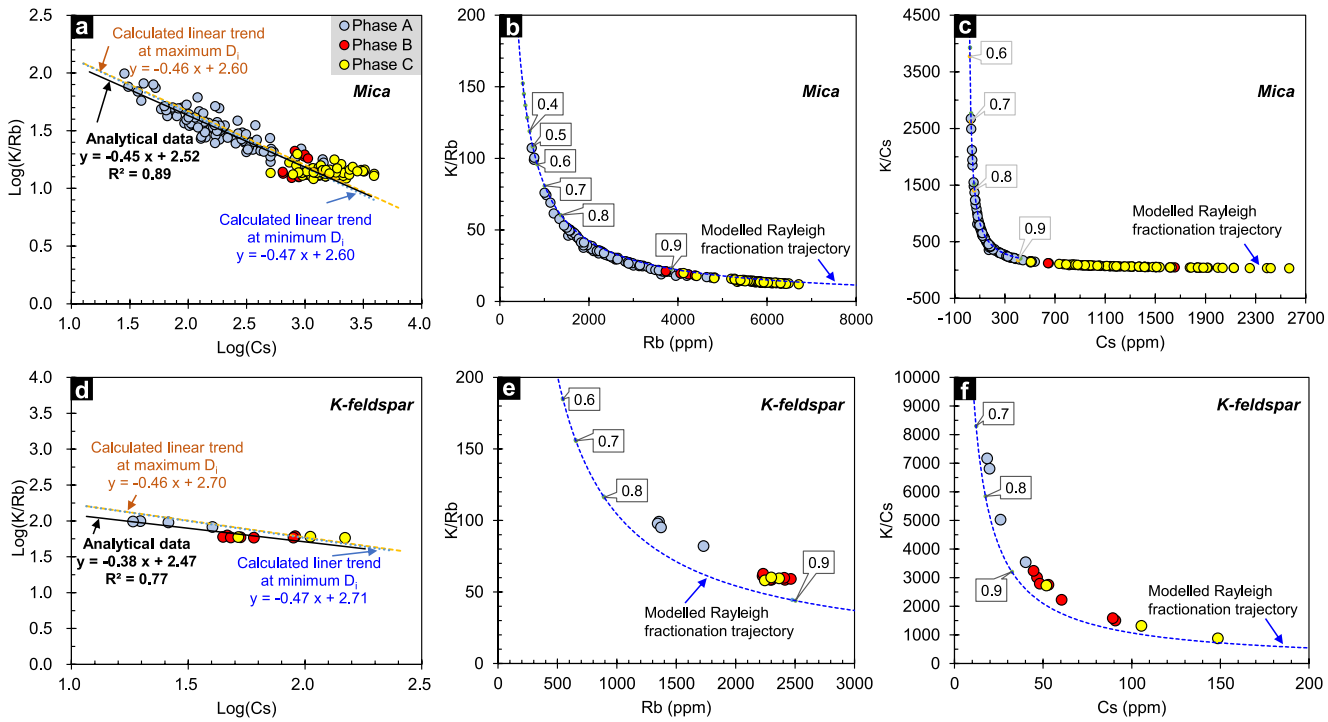


**Figure 5.** Plots of K/Rb versus Cs in trioctahedral micas (a) and K-feldspars (d) for the granites of the different phases of the Xihushan pluton. Plots of K/Cs versus Cs and K/Rb versus Rb plots for trioctahedral micas (b and c) and K-feldspars (e and f) from the three phases of granites in the Xihuashan pluton. The numbers on the modeled Rayleigh fractionation curve denote the mass fraction of melt remaining.

and Hf contents follow a theoretical curve for Zr/Hf fractionation of zircon developed for rare-metal granites globally (Wang et al., 2000) (Figure S6 in Supporting Information S1). These compositional variations of zircon are produced by fractional crystallization (Breiter & Škoda, 2017; Linnen & Keppler, 2002) and are effective proxies of the degree of magmatic differentiation. Thus, magmatic differentiation is not only documented by the chemical compositions of bulk rocks but also evident in those of minerals.

### 5.2. Li Isotope Fractionation During Magmatic Differentiation

The most evolved granites in the Xihuashan and Yaogangxian plutons have the highest Li contents and $\delta^7$Li values. The $\delta^7$Li values of the rock-forming minerals (quartz, plagioclase, K-feldspar, trioctahedral mica) and accessory zircon are all elevated in Phases B and C relative to Phase A, consistent with the trend of the bulk rocks. Trioctahedral mica, K-feldspar, and zircon from granites in the Xihuashan pluton display continuous evolution of chemical compositions from Phases A to C that correlates with their $\delta^7$Li values. All these indicate that sizable Li isotope fractionation is controlled by magmatic differentiation, which promotes the gradual enrichment of $^7$Li in residual melts.

Experimental studies suggest that $^6$Li diffuses up to 3% more rapidly than $^7$Li in the melt due to their large mass difference (Beck et al., 2006; Richter et al., 2003). Thus, the kinetic fractionation effect caused by diffusion during mineral crystallization could potentially lead to a heavier Li isotopic composition in the residual melt as $^6$Li diffuses faster than $^7$Li into crystallizing minerals, associated with preferential removal of $^6$Li from the melt during magmatic differentiation (Beck et al., 2006). In situ Li isotope analyses using secondary ion mass spectrometer revealed that Li isotope compositions of zircons are highly variable in granites (Gao et al., 2015). The considerable isotopic variation in zircon appears to have resulted from intracrystalline diffusion occurring on the micron scale (Dohmen et al., 2010; Gao et al., 2015). It was previously proposed by Li et al. (2018) that if the interaction between mica and Li-bearing fluid happens rather rapidly, the diffusion of Li from mica (primary Li carrier) into fluid can cause the granites to be more enriched in heavy Li isotopes because $^6$Li diffuses faster than the $^7$Li from minerals to fluid; however, this cannot explain the higher Li concentration associated with heavier Li in late-stage granites. In the Xihuashan pluton, the $\delta^7$Li values of quartz, plagioclase, and mica display positive correlations (Figure 7), which is unlikely the result of disequilibrium Li isotope fractionation caused by diffusion.

**Table 3**
*Li Concentration and Li Isotopic Compositions of Mineral Separated From Granites and Greisen of the Xihuashan Pluton*

| Mineral/ sample | Quartz | | | Plagioclase | | | Mica | | | K-feldspar | | | Zircon | | | Garnet | | | ΔLi | ΔLi | ΔLi |
|---|---|---|---|---|---|---|---|---|---|---|---|---|---|---|---|---|---|---|---|---|---|
| | Li [ppm] | $\delta^7$Li (‰) | 2SD | Li [ppm] | $\delta^7$Li (‰) | 2SD | Li [ppm] | $\delta^7$Li (‰) | 2SD | Li [ppm] | $\delta^7$Li (‰) | 2SD | Li [ppm] | $\delta^7$Li (‰) | 2SD | Li [ppm] | $\delta^7$Li (‰) | 2SD | Quartz-plagioclase | Quartz-mica | Plagioclase-mica |
| Phase A | – | – | – | – | – | – | – | – | – | – | – | – | – | – | – | – | – | – | 18.0 | 15.3 | −2.8 |
| XHS-5 | 11.1 | 14.0 | 0.07 | 16.0 | −4.0 | 0.19 | 2897 | −1.3 | 0.18 | 41.9 | −4.2 | 0.03 | 24.0 | −3.3 | 0.32 | – | – | – | 16.2 | 15.0 | −1.2 |
| XHS-6 | 24.0 | 13.7 | 0.02 | 26.6 | −2.4 | 0.20 | 2978 | −1.2 | 0.09 | 9.60 | 0.5 | 0.13 | – | – | – | – | – | – | 16.8 | 15.1 | −1.7 |
| XHS-18 | 24.1 | 13.8 | 0.27 | 41.2 | −3.0 | 0.02 | 3115 | −1.4 | 0.23 | – | – | – | – | – | – | – | – | – | 18.0 | 15.6 | −2.3 |
| XHS-21 | 18.9 | 13.8 | 0.31 | 19.2 | −4.2 | 0.11 | 3002 | −1.9 | 0.16 | – | – | – | – | – | – | – | – | – | – | – | – |
| Phase B | – | – | – | – | – | – | – | – | – | – | – | – | – | – | – | – | – | – | 15.2 | 16.8 | 1.6 |
| XHS-9 | 18.6 | 17.4 | 0.22 | 24.4 | 2.2 | 0.46 | 3557 | 0.6 | 0.48 | – | – | – | 49.4 | 1.6 | 0.25 | 581 | −3.1 | 0.30 | 17.0 | 16.8 | −0.1 |
| XHS-12 | 18.6 | 16.4 | 0.11 | 16.7 | −0.6 | 0.05 | 3130 | −0.4 | 0.09 | – | – | – | – | – | – | 564 | −2.5 | 0.22 | 17.0 | 18.3 | 1.3 |
| XHS-16 | 21.0 | 18.3 | 0.13 | 24.2 | 1.3 | 0.29 | 2955 | 0.0 | 0.03 | – | – | – | 26.4 | 1.4 | 0.39 | 541 | −2.6 | 0.42 | 18.7 | 17.0 | −1.7 |
| XHS-20 | 16.5 | 17.8 | 0.20 | 40.8 | −0.9 | 0.27 | 3995 | 0.8 | 0.19 | – | – | – | 40.9 | −1.1 | 0.32 | 486 | −3.6 | 0.05 | 15.5 | 16.3 | 0.8 |
| DP-3 | 31.4 | 15.9 | 0.37 | 26.1 | 0.4 | 0.22 | 3416 | −0.4 | 0.43 | – | – | – | – | – | – | – | – | – | – | – | – |
| Phase C | – | – | – | – | – | – | – | – | – | – | – | – | – | – | – | – | – | – | 16.8 | 16.0 | −0.8 |
| XHS-7 | 23.3 | 16.8 | 0.06 | 26.3 | 0.0 | 0.43 | 4537 | 0.8 | 0.10 | – | – | – | – | – | – | 508 | −2.2 | 0.22 | 18.6 | 17.8 | −0.8 |
| XHS-10 | 23.2 | 18.9 | 0.06 | 25.0 | 0.2 | 0.54 | 6641 | 1.0 | 0.09 | 13.99 | 2.71 | 0.14 | – | – | – | 568 | −2.7 | 0.09 | – | – | – |
| Greisen | – | – | – | – | – | – | – | – | – | – | – | – | – | – | – | – | – | – | – | 3.0 | 3.0 |
| XHS-14 | – | – | – | – | – | – | 5887 | −3.0 | 0.28 | – | – | – | – | – | – | – | – | – | – | – | – |

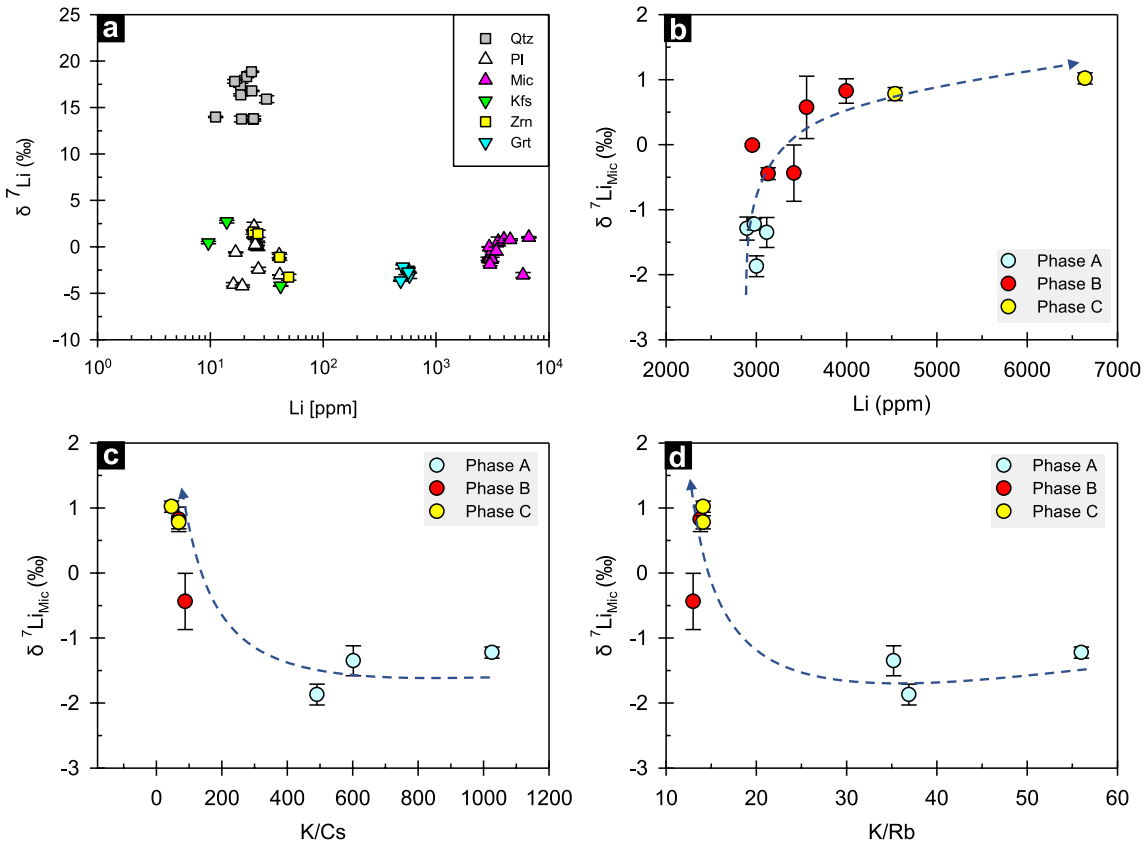


**Figure 6.** Plot of Li concentrations versus Li isotope compositions for all minerals from the Xihuashan pluton (a). Binary plots show the relationship between the Li isotope and chemical compositions of trioctahedral mica from granites in the Xihuashan pluton (b-d). The average K/Cs and K/Rb ratios are from EPMA and LA-ICPMS data. Abbreviations: quartz (Qtz); plagioclase (Pl); Mica (mic); K-feldspar (Kfs); zircon (Zrn); garnet (Grt).

Lithium is mainly contained within mica in peraluminous granites, with lesser amounts in cordierite and garnet (Magna et al., 2016). In these minerals, Li is octahedrally coordinated (Liu et al., 2018; Magna et al., 2016). In contrast, Li is tetrahedrally coordinated in granitic melts (Soltay & Henderson, 2005). Teng et al. (2006) and Magna et al. (2016) proposed that $^{6}$Li favors a high-coordination site, whereas $^{7}$Li preferentially incorporates into a lower-coordination site during equilibrium fractionation. Thus, with continuous removal of these Li-bearing minerals, there would be a corresponding increase in the $\delta^{7}$Li value of the residual granitic magma. Indeed, the $^{7}$Li/$^{6}$Li ratios are elevated in the late-stage granites of both the Xihuashan and Yaogangxian plutons, consistent with equilibrium Li isotope fractionation during magmatic differentiation. Moreover, the $\Delta Li_{plagioclase\text{-}mica}$ and $\Delta Li_{quartz\text{-}mica}$ values are elevated in the late-stage granites (Table 3), which can be explained by the lowered temperatures and consistent with the equilibrium Li isotope fractionation occurring among minerals. Therefore, it was more likely that equilibrium fractionation accounts for Li isotopic variations among different stages. However, it is noteworthy that although the equilibrium fractionation between melt and crystallized minerals dominates the Li isotopic variations among different phases of granites, other processes, such as kinetic fractionation between mineral and fluid or fluid-rock interaction, cannot be ruled out as secondary processes.

### 5.3. The Quantitative Model of Magmatic Differentiation Control on Li Isotope Fractionation

To quantitatively assess the coupled relationship between Li isotope composition and the different phases of granites, knowledge of the extent of differentiation of the different phases is essential. Hulsbosch et al. (2014) demonstrated that alkali metals in K-feldspar and mica are sensitive monitors of granitic magma evolution, as the variation of the alkali metal concentrations in these minerals can accurately indicate the degree of differentiation ($F$) of the residual melt. If a series of compositions of a mineral ($i$) is generated by Rayleigh crystal fractionation, as expressed by Equation 1, it can be inferred that log (Cs) and log (K/Rb) in mineral ($i$) should have a linear relationship [Equation 3]. The bulk partition coefficient $D_j$ of the mineral assemblage removed determines the slope

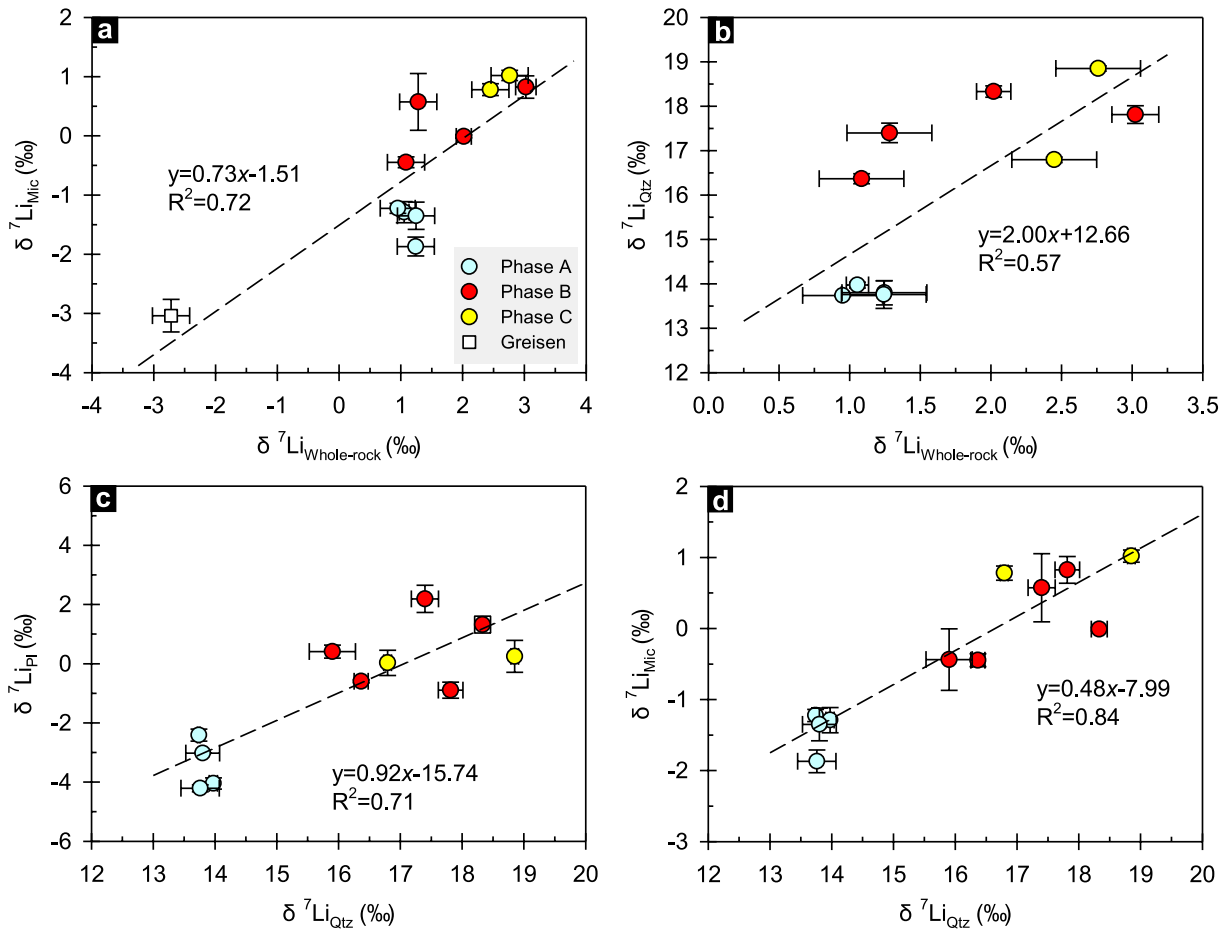


**Figure 7.** Plots of bulk-rock $\delta^7$Li values versus mica $\delta^7$Li values (a), bulk-rock $\delta^7$Li values versus plagioclase $\delta^7$Li values (b), quartz $\delta^7$Li values versus plagioclase $\delta^7$Li values (c) and quartz $\delta^7$Li values versus mica $\delta^7$Li values (d). Abbreviation: mica (mic), quartz (qtz), plagioclase (Pl).

of this line ($A$) [Equation 4]. The intercept ($B$) of the line depends on the partition coefficient $k_{d,i,j}$ of element $j$ between mineral $i$ and initial melt [Equation 5].

$$\frac{C_{\mathrm{liq},j}}{C_o} = F^{(D_j-1)} \tag{1}$$

$$C_{i,j} = C_o \times k_{d,ij} \times F^{(D_j-1)} \tag{2}$$

$$\log\left(\frac{C_{i,k}}{C_{i,Rb}}\right) = A \times \log(C_{i,Cs}) + B \tag{3}$$

$$\mathrm{A} = \frac{D_K - D_{Rb}}{D_{Cs} - 1} \tag{4}$$

$$\mathrm{B} = \log\left(\frac{C_{o,K} \times K_{d,i,K}}{C_o \times K_{d,i,Rb}}\right) - A \times \log(C_{o,Rb} \times K_{d,i,Cs}) \tag{5}$$

$F$: mass fraction of melt;
$C_{o,j}$: concentration of element $j$ in initial melt;
$C_{i,j}$, $C_{\mathrm{liq},j}$: element $j$ concentrations in mineral $i$ and residual melt;
$k_{d,i,j}$: mineral-melt partition coefficient of element $j$;
$D_j$: bulk mineral-melt partition coefficient of element $j$, $D_j = \sum_i x_i \times k_{d,i,j}$;
$x_i$: mass fraction for mineral $j$, $\sum_i x_i = 1$.

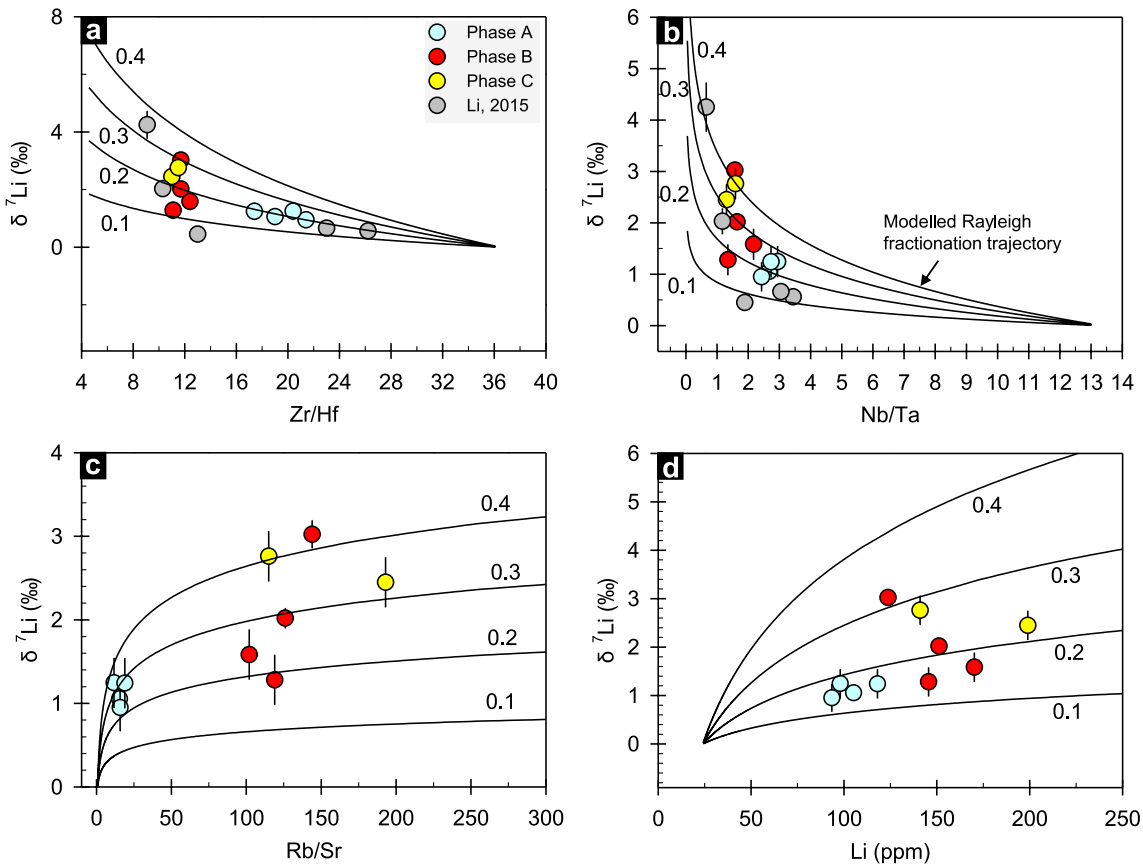


**Figure 8.** Modeling shows the Li isotopic and trace elemental evolution of residual magmas during a Rayleigh process. The equations and related parameters from Teng et al. (2006): $\delta^7Li_m = (\delta^7Li_i + 1{,}000)f^{(\alpha-1)} - 1{,}000$; $C_m = C_iF^{(D-1)}$; $\alpha = (^7Li/^6Li)_{mineral}/(^7Li/^6Li)_{melt}$; $D_{Li} = Li_{mineral}/Li_{melt}$; $f$ = the fraction of Li remaining in the melts; $F$ = fraction of remaining melt. $m$ = remaining melt; $i$ = initial melt. The numbers on the curves represent different bulk partition coefficients of Li ($D_{Li}$). The parameters for modeling chemical compositions are referred to Table S5 in Supporting Information S2. The curves denote calculated melt evolution using variable $D$ values.

Mineral/melt partition coefficients for alkali metals in K-feldspar and mica crystallizing from granitic melts have been well-documented (see Table S5 in Supporting Information S2). Previous studies have suggested that the granites from the Xihuashan and Yaogangxian plutons formed from pelite-derived magmas in the upper continental crust (Dong et al., 2014; Yang et al., 2018), so the average composition of the upper continental crust in South China (31,244 ppm K, 26 ppm Cs, and 245 ppm Rb; Chi & Yan, 2007; Rudnick & Gao, 2003), is used to represent the initial composition of the magma for modeling the differentiation of the granites of the Xihuashan pluton. The estimated relative proportions of the removed mineral assemblage are similar to those for a near-eutectic mineral assemblage (Table S5 in Supporting Information S2). The linear relationships for log (K/Rb) and log (Cs) are expected for trioctahedral mica (Figure 5a) and K-feldspar (Figure 5d) and agree well with the theoretical calculation by using the alkali fractionation model mentioned above. It is noted that the slope ($A$) and intercept ($B$) vary slightly among the different granite phases, which is most likely due to different mineral compositions in the assemblage removed from the melt. This shows that the estimated values of the parameters $K_{d,j}$, $C_{o,j}$, $D_j$ and mineral assemblage are appropriate and that the differentiation model can characterize the evaluation of the melt of the Xihuashan pluton. Comparisons of the analyzed alkali metal concentration data (K/Rb vs. Rb and K/Cs vs. Cs) with the models for mica and K-feldspar (Figures 5b, 5c, 5e, and 5f) show that the Phase Agranites in the Xihuashan pluton crystallized from the residues of parental magma that had undergone 50%–90% crystallization, and Phases B and C granites represent the products of the magma with >90% crystallization. To further test the model, we also evaluated the compositional changes of REEs, U, and Th in zircon of different phases, which yielded melt fractions similar to those estimated using alkali metal in mica and K-feldspar (Figure S6 in Supporting Information S1).

With continuous crystallization, the changes in Li isotope compositions of the remaining magmas can be modeled by the Rayleigh fractionation model (Figure 8). The initial composition of parental magma was set as 24 ppm for Li and 0.0‰ for $\delta^7Li$ (Rudnick & Gao, 2003; Teng et al., 2004). A fractionation factor ($\alpha$) between

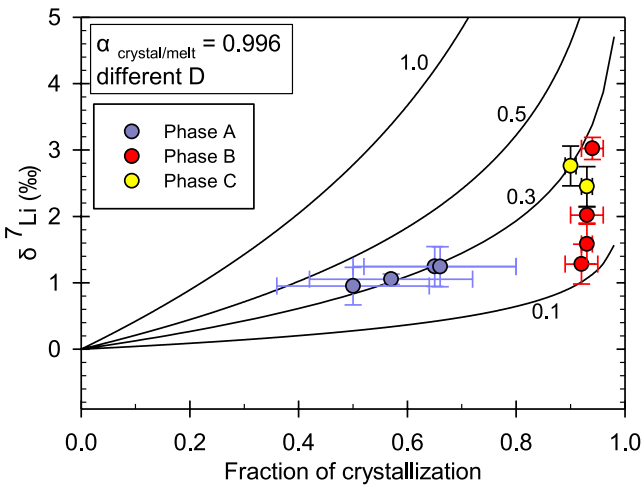


**Figure 9.** Binary plot showing the correlation between lithium isotopic fractionation and the degrees of magmatic differentiation. The degree of differentiation of the granites was calculated according to the Rb content of trioctahedral mica and the U content of the zircon. The error bar is twice the standard deviation (2SD).

the crystallizing mineral assemblage and the magma [$\alpha_{minerals/melt} = (^7Li/^6Li)_{mineral}/(^7Li/^6Li)_{melt}$] is assumed to be 0.996, which is extrapolated based on the Rayleigh distillation model of Harney Peak Granites (Teng et al., 2006). The bulk partition coefficient of Li ($D_{Li}$) for the mineral assemblage ranges from 0.1 to 0.5 (Table S5 in Supporting Information S2). As seen in Figure 8, the Rayleigh model shows that the $\delta^7$Li values gradually increase with evolving differentiation in the residual magma, with the late stage of magma significantly enriched in $^7$Li. There is a concomitant variation between the Li isotope ratio and chemical composition of the residual magma (e.g., Zr/Hf and Nb/Ta), consistent with analyzed data of the granites. Furthermore, on the plot of Li isotopes versus the degrees of differentiation, which were obtained using the Rb contents in trioctahedral mica and the U contents in zircon, the $\delta^7$Li values of the three phases granites in the Xihuashan pluton are identical within the uncertainty to the theoretically modeled value by assuming $D_{Li}$ value of 0.1–0.5 (Figure 9). All samples fail to plot on a single curve, which could be the result of slight variations in $D_{Li}$ during magmatic differentiation.

In summary, our modeling calculations support measurable Li isotope fractionation during magmatic differentiation (crystal-melt). Quantitative modeling of the differentiation of the granites from the Xihuashan pluton indicates that the Li isotope compositions predicted using this modeling are indistinguishable from the analyzed Li isotope compositions. This modeling also shows that significant Li isotope fractionation will only be observed in granites that have undergone high degrees of magmatic differentiation.

### 5.4. Implications for Rare-Metal Mineralization

Granites from the Xihuashan and Yaogangxian plutons show convincing evidence of Li isotope fractionation with higher $\delta^7$Li values in the more evolved late-stage granites. We propose that the elevated $\delta^7$Li records intense magmatic differentiation, which promoted the mineralization of rare metals.

The late-stage granites contain abundant fluorite and xenotime. In Phases B and C of Xihuashan pluton, trioctahedral micas are enriched in rare metals such as W, Sn, and Li (Figure S4 in Supporting Information S1) and have high P contents. All these observations indicate that with the magmatic differentiation, the residual melts develop very high contents of volatile components (e.g., F and P) and rare metals (e.g., W, Sn). Intense magmatic differentiation would have favored the enrichment of fluxing elements, which would have increased the solubility of rare metals in magmas, thereby ensuring that the fluids exsolved from the most evolved granites contained the concentrations of these metals required to form economic deposits.

## 6. Conclusions

1. Lithium isotope fractionation occurs in rare-metal-rich granites. Intense magmatic differentiation can produce heavier Li isotopic composition in the late stage. Greisen samples generally have much lower $\delta^7$Li values than their host granites, which can be attributed to fluid exsolution.
2. Different minerals' chemical compositions and Li isotope systematics uniformly indicate that fractional crystallization significantly affects Li isotope behavior in granites and promotes $^7$Li enrichment in residual melts. The systematically elevated $\delta^7$Li values in rare-metal granites result from equilibrium Li isotope fractionation and reflect high degrees of magmatic differentiation.
3. Extreme magmatic differentiation generated late-phase granites enriched in elements, such as Li, F, and P, which facilitates the formation of rare-metal deposits. Thus, the behavior of Li isotopes in rare-metal granites provides new insights into magmatic differentiation and rare-metal mineralization.

## Data Availability Statement

All major, minor, and trace element and Li isotope data for Yaogangxian and Xihuashan used in this study are accessible in the open-access Zenodo data repository https://doi.org/10.5281/zenodo.7324761 available from the publication date.

**Acknowledgments**
This research was supported by the National Science Foundation of China (Grant 42073046). Additional support was provided from the CAS "Light of West China" Program to Jie-Hua Yang, K.C.Wong Education Foundation (Grant GJTD-2020-13) and the Innovation and Entrepreneurship Funding of High-Level Overseas Talents of Guizhou Province (Jie-Hua Yang, [2020]03). We thank the geologists of the Xihuashan Mine and the Yaogangxian Mine for their help during our field work. HC thanks LDEO and Columbia Climate School for research support. We greatly appreciate Prof. Paul B. Tomascak and the anonymous reviewer for constructive suggestions that helped to significantly improve this draft. Special thanks are extended to Prof. Yi-Lin Xiao for his help with analyses and technical assistance.

## References

Barnes, E. M., Weis, D., & Groat, L. A. (2012). Significant Li isotope fractionation in geochemically evolved rare element-bearing pegmatites from the little Nahanni Pegmatite Group, NWT, Canada. *Lithos*, *132–133*, 21–36. https://doi.org/10.1016/j.lithos.2011.11.014

Beck, P., Chaussidon, M., Barrat, J. A., Gillet, P., & Bohn, M. (2006). Diffusion induced Li isotopic fractionation during the cooling of magmatic rocks: The case of pyroxene phenocrysts from nakhlite meteorites. *Geochimica et Cosmochimica Acta*, *70*(18), 4813–4825. https://doi.org/10.1016/j.gca.2006.07.025

Bell, E. A., Boehnke, P., Barboni, M., & Harrison, T. M. (2019). Tracking chemical alteration in magmatic zircon using rare Earth element abundances. *Chemical Geology*, *510*, 56–71. https://doi.org/10.1016/j.chemgeo.2019.02.027

Breiter, K., & Škoda, R. (2017). Zircon and whole-rock Zr/Hf ratios as markers of the evolution of granitic magmas: Examples from the Teplice caldera (Czech Republic/Germany). *Mineralogy and Petrology*, *111*(4), 435–457. https://doi.org/10.1007/s00710-017-0509-z

Chan, L.-H., Alt, J. C., & Teagle, D. A. H. (2002). Lithium and lithium isotope profiles through the upper oceanic crust: A study of seawater–basalt exchange at ODP sites 504B and 896A. *Earth and Planetary Science Letters*, *201*(1), 187–201. https://doi.org/10.1016/s0012-821x(02)00707-0

Chappell, B. W., White, A. J. R., Williams, I. S., & Wyborn, D. (2004). Low- and high-temperature granites. *Earth & Environmental Science Transactions of the Royal Society of Edinburgh*, *95*(1–2), 125–140. https://doi.org/10.1017/s0263593300000973

Chen, B., Gu, H.-o., Chen, Y., Sun, K., & Chen, W. (2018). Lithium isotope behavior during partial melting of metapelites from the Jiangnan Orogen, South China: Implications for the origin of REE tetrad effect of F-rich granite and associated rare-metal mineralization. *Chemical Geology*, *483*, 372–384. https://doi.org/10.1016/j.chemgeo.2018.03.002

Chen, Y.-R. (1988). Geological and geochemical characteristics and diagenetic-minerogenetic processes of Yaogangxian granite (in Chinese with English abstract). *Mineral Resources and Geology*, *2*(1), 62–72.

Chi, Q., & Yan, M. (2007). *Handbook of elemental abundance for applied geochemistry (in Chinese)* (pp. 98–115). Geological Publishing House.

Deveaud, S., Millot, R., & Villaros, A. (2015). The Genesis of LCT-type granitic pegmatites, as illustrated by lithium isotopes in micas. *Chemical Geology*, *411*, 97–111. https://doi.org/10.1016/j.chemgeo.2015.06.029

Dohmen, R., Kasemann, S. A., Coogan, L., & Chakraborty, S. (2010). Diffusion of Li in olivine. Part I: Experimental observations and a multi species diffusion model. *Geochimica et Cosmochimica Acta*, *74*(1), 274–292. https://doi.org/10.1016/j.gca.2009.10.016

Dong, S.-H., Bi, X.-W., Hu, R.-Z., & Chen, Y.-W. (2014). Petrogenesis of the Yaogangxian granites and implications for W mineralization, Hunan Province (in Chinese with English abstract). *Acta Petrologica Sinica*, *30*(9), 2749–2765.

Gao, Y., & Casey, J. F. (2012). Lithium isotope composition of ultramafic geological reference materials JP-1 and DTS-2. *Geostandards and Geoanalytical Research*, *36*(1), 75–81. https://doi.org/10.1111/j.1751-908x.2011.00117.x

Gao, Y.-Y., Li, X. H., Griffin, W. L., Tang, Y. J., Pearson, N. J., Liu, Y., et al. (2015). Extreme lithium isotopic fractionation in three zircon standards (Plešovice, Qinghu and Temora). *Scientific Reports*, *5*(1), 16878. https://doi.org/10.1038/srep16878

Guo, C. L., Chen, Y. C., Zeng, Z. L., & Lou, F. S. (2012). Petrogenesis of the Xihuashan granites in southeastern China: Constraints from geochemistry and in-situ analyses of zircon U-Pb-Hf-O isotopes. *Lithos*, *148*, 209–227. https://doi.org/10.1016/j.lithos.2012.06.014

Hanchar, J. M., Finch, R. J., Hoskin, P. W., Watson, E. B., Cherniak, D. J., & Mariano, A. N. (2001). Rare Earth elements in synthetic zircon: Part 1. Synthesis, and rare Earth element and phosphorus doping. *American Mineralogist*, *86*(5–6), 667–680. https://doi.org/10.2138/am-2001-5-607

Holycross, M., Watson, E., Richter, F., & Villeneuve, J. (2018). Diffusive fractionation of Li isotopes in wet, highly silicic melts. *Geochemical Perspectives Letters*, *6*, 39–42. https://doi.org/10.7185/geochemlet.1807

Hulsbosch, N., Boiron, M.-C., Dewaele, S., & Muchez, P. (2016). Fluid fractionation of tungsten during granite–pegmatite differentiation and the metal source of peribatholitic W quartz veins: Evidence from the Karagwe-Ankole Belt (Rwanda). *Geochimica et Cosmochimica Acta*, *175*, 299–318. https://doi.org/10.1016/j.gca.2015.11.020

Hulsbosch, N., Hertogen, J., Dewaele, S., André, L., & Muchez, P. (2014). Alkali metal and rare Earth element evolution of rock-forming minerals from the Gatumba area pegmatites (Rwanda): Quantitative assessment of crystal-melt fractionation in the regional zonation of pegmatite groups. *Geochimica et Cosmochimica Acta*, *132*, 349–374. https://doi.org/10.1016/j.gca.2014.02.006

Jochum, K. P., Nohl, L., Herwig, K., Lammel, E., Stoll, B., & Hofmann, A. W. (2005). GeoReM: A new geochemical database for reference materials and isotopic standards. *Geostandards and Geoanalytical Research*, *29*(3), 333–338. https://doi.org/10.1111/j.1751-908x.2005.tb00904.x

Li, J. (2015). Mineralogical constraints on magmatic and hydrothermal evolutions of the esozoic rare-metal granites in South China (in Chinese with English Abstract), PhD Thesis, (pp. 80–81). Guangzhou Institute of Geochemistry, Chinese Academy of Sciences.

Li, J., Huang, X. L., Wei, G. J., Liu, Y., Ma, J. L., Han, L., & He, P. L. (2018). Lithium isotope fractionation during magmatic differentiation and hydrothermal processes in rare-metal granites. *Geochimica et Cosmochimica Acta*, *240*, 64–79. https://doi.org/10.1016/j.gca.2018.08.021

Li, S.-T., Wang, J. B., Zhu, X. Y., Wang, Y. L., Han, Y., & Guo, N. N. (2011). Chronological characteristics of the Yaogangxian composite pluton in Hunan Province. *Geology and Exploration*, *47*(02), 143–150. (in Chinese with English abtract).

Linnen, R. L., & Keppler, H. (2002). Melt composition control of Zr/Hf fractionation in magmatic processes. *Geochimica et Cosmochimica Acta*, *66*(18), 3293–3301. https://doi.org/10.1016/s0016-7037(02)00924-9

Liu, H., Xiao, Y., Sun, H., Tong, F., Heuser, A., Churikova, T., & Worner, G. (2020). Trace elements and Li isotope compositions across the Kamchatka arc: Constraints on slab-derived fluid sources. *Journal of Geophysical Research: Solid Earth*, *125*(5), e2019JB019237. https://doi.org/10.1029/2019jb019237

Liu, S., Li, Y., Liu, J., Ju, Y., Liu, J., Yang, Z., & Shi, Y. (2018). Equilibrium lithium isotope fractionation in Li-bearing minerals. *Geochimica et Cosmochimica Acta*, *235*, 360–375. https://doi.org/10.1016/j.gca.2018.05.029

Liu, Y., Gao, S., Hu, Z., Gao, C., Zong, K., & Wang, D. (2010). Continental and oceanic crust recycling-induced melt–peridotite interactions in the trans-North China Orogen: U–Pb dating, Hf isotopes and trace elements in zircons from mantle Xenoliths. *Journal of Petrology*, *51*(1–2), 537–571. https://doi.org/10.1093/petrology/egp082

London, D. (2005). Granitic pegmatites: An assessment of current concepts and directions for the future. *Lithos*, *80*(1), 281–303. https://doi.org/10.1016/j.lithos.2004.02.009

Luth, W. C., Jahns, R. H., & Tuttle, O. F. (1964). The granite system at pressures of 4 to 10 kilobars. *Journal of Geophysical Research*, *69*(4), 759–773. https://doi.org/10.1029/jz069i004p00759

Magna, T., Novak, M., Cempirek, J., Janousek, V., Ullmann, C. V., & Wiechert, U. (2016). Crystallographic control on lithium isotope fractionation in Archean to Cenozoic lithium-cesium-tantalum pegmatites. *Geology*, *44*(8), 655–658. https://doi.org/10.1130/g37712.1

Magna, T., Wiechert, U., & Halliday, A. N. (2006). New constraints on the lithium isotope compositions of the Moon and terrestrial planets. *Earth and Planetary Science Letters*, *243*(3–4), 336–353. https://doi.org/10.1016/j.epsl.2006.01.005

Mao, J., Ouyang, H. G., Song, S. W., Santosh, M., Yuan, S. D., Zhou, Z. H., et al. (2019). *Geology and metallogeny of tungsten and tin deposits in China* (Vol. 22, pp. 411–482). Society of Economic Geologists, Inc. Special Publication.

Marschall, H. R., Pogge von Strandmann, P. A. E., Seitz, H.-M., Elliott, T., & Niu, Y. (2007). The lithium isotopic composition of orogenic eclogites and deep subducted slabs. *Earth and Planetary Science Letters*, *262*(3), 563–580. https://doi.org/10.1016/j.epsl.2007.08.005

Penniston-Dorland, S., Liu, X. M., & Rudnick, R. L. (2017). Lithium isotope geochemistry. *Reviews in Mineralogy and Geochemistry*, *82*(1), 165–217. https://doi.org/10.2138/rmg.2017.82.6

Pistiner, J. S., & Henderson, G. M. (2003). Lithium-isotope fractionation during continental weathering processes. *Earth and Planetary Science Letters*, *214*(1–2), 327–339. https://doi.org/10.1016/s0012-821x(03)00348-0

Piwinskii, A. J. (1973). Experimental studies of granitoids from the central and southern coast ranges, California. *Tschermaks Mineralogische und Petrographische Mitteilungen*, *20*(2), 107–130. https://doi.org/10.1007/bf01081387

Qi, L., Hu, J., & Gregoire, D. C. (2000). Determination of trace elements in granites by inductively coupled plasma mass spectrometry. *Talanta*, *51*(3), 507–513. https://doi.org/10.1016/s0039-9140(99)00318-5

Qiu, L., Rudnick, R. L., McDonough, W. F., & Bea, F. (2011). The behavior of lithium in amphibolite-to granulite-facies rocks of the Ivrea–Verbano Zone, NW Italy. *Chemical Geology*, *289*(1), 76–85. https://doi.org/10.1016/j.chemgeo.2011.07.014

Richter, F. M., Davis, A. M., DePaolo, D. J., & Watson, E. B. (2003). Isotope fractionation by chemical diffusion between molten basalt and rhyolite. *Geochimica et Cosmochimica Acta*, *67*(20), 3905–3923. https://doi.org/10.1016/s0016-7037(03)00174-1

Rudnick, R., & Gao, S. (2003). Composition of the continental crust. In H. D. Holland, & K. K. Turekian (Eds.), *Treatise on geochemistry* (Vol. 3, pp. 1–64). Elsevier.

Rudnick, R. L., Tomascak, P. B., Njo, H. B., & Gardner, L. R. (2004). Extreme lithium isotopic fractionation during continental weathering revealed in saprolites from South Carolina. *Chemical Geology*, *212*(1), 45–57. https://doi.org/10.1016/j.chemgeo.2004.08.008

Schuessler, J. A., Schoenberg, R., & Sigmarsson, O. (2009). Iron and lithium isotope systematics of the Hekla volcano, Iceland—Evidence for Fe isotope fractionation during magma differentiation. *Chemical Geology*, *258*(1), 78–91. https://doi.org/10.1016/j.chemgeo.2008.06.021

Soltay, L. G., & Henderson, G. S. (2005). The structure of lithium-containing silicate and germanate glasses. *The Canadian Mineralogist*, *43*(5), 1643–1651. https://doi.org/10.2113/gscanmin.43.5.1643

Stepanov, A., Mavrogenes, A. J., Meffre, S., & Davidson, P. (2014). The key role of mica during igneous concentration of tantalum. *Contributions to Mineralogy and Petrology*, *167*(6), 1–8. https://doi.org/10.1007/s00410-014-1009-3

Sun, H., Gao, Y., Xiao, Y., Gu, H.-O., & Casey, J. F. (2016). Lithium isotope fractionation during incongruent melting: Constraints from post-collisional leucogranite and residual enclaves from Bengbu Uplift, China. *Chemical Geology*, *439*, 71–82. https://doi.org/10.1016/j.chemgeo.2016.06.004

Tang, M., Rudnick, R. L., & Chauvel, C. (2014). Sedimentary input to the source of Lesser Antilles lavas: A Li perspective. *Geochimica et Cosmochimica Acta*, *144*, 43–58. https://doi.org/10.1016/j.gca.2014.09.003

Teng, F. Z., McDonough, W., Rudnick, R., Dalpe, C., Tomascak, P., Chappell, B., & Gao, S. (2004). Lithium isotopic composition and concentration of the upper continental crust. *Geochimica et Cosmochimica Acta*, *68*(20), 4167–4178. https://doi.org/10.1016/j.gca.2004.03.031

Teng, F.-Z., McDonough, W. F., Rudnick, R. L., Walker, R. J., & Sirbescu, M.-L. C. (2006). Lithium isotopic systematics of granites and pegmatites from the Black Hills, South Dakota. *American Mineralogist*, *91*(10), 1488–1498. https://doi.org/10.2138/am.2006.2083

Teng, F.-Z., McDonough, W. F., Rudnick, R. L., & Wing, B. A. (2007). Limited lithium isotopic fractionation during progressive metamorphic dehydration in metapelites: A case study from the Onawa contact aureole, Maine. *Chemical Geology*, *239*(1–2), 1–12. https://doi.org/10.1016/j.chemgeo.2006.12.003

Tischendorf, G., Gottesmann, B., Förster, H., & Trumbull, R. B. (1997). On Li-bearing micas: Estimating Li from electron microprobe analyses and an improved diagram for graphical representation. *Mineralogical Magazine*, *61*(6), 809–834. https://doi.org/10.1180/minmag.1997.061.409.05

Tomascak, P. B. (2004). Developments in the understanding and application of lithium isotopes in the Earth and planetary Sciences. *Reviews in Mineralogy and Geochemistry*, *55*(1), 153–195. https://doi.org/10.2138/gsrmg.55.1.153

Tomascak, P. B., Magna, T., & Dohmen, R. (2016). *Advances in lithium isotope geochemistry*. Springer.

Tomascak, P. B., Tera, F., Helz, R. T., & Walker, R. J. (1999). The absence of lithium isotope fractionation during basalt differentiation: New measurements by multicollector sector ICP-MS. *Geochimica et Cosmochimica Acta*, *63*(6), 907–910. https://doi.org/10.1016/s0016-7037(98)00318-4

Vigier, N., Gislason, S. R., Burton, K. W., Millot, R., & Mokadem, F. (2009). The relationship between riverine lithium isotope composition and silicate weathering rates in Iceland. *Earth and Planetary Science Letters*, *287*(3–4), 434–441. https://doi.org/10.1016/j.epsl.2009.08.026

Vlastélic, I., Staudacher, T., Bachelery, P., Telouk, P., Neuville, D., & Benbakkar, M. (2011). Lithium isotope fractionation during magma degassing: Constraints from silicic differentiates and natural gas condensates from Piton de la Fournaise volcano (Réunion Island). *Chemical Geology*, *284*(1), 26–34. https://doi.org/10.1016/j.chemgeo.2011.02.002

von Strandmann, P., Desrochers, A., Murphy, M., Finlay, A., Selby, D., & Lenton, T. (2017). Global climate stabilisation by chemical weathering during the Hirnantian glaciation. *Geochemical Perspectives Letters*, *3*(2), 230–236. https://doi.org/10.7185/geochemlet.1726

Wang, R. C., Zhao, G. T., Lu, J. J., Chen, X. M., Xu, S. J., & Wang, D. Z. (2000). Chemistry of Hf-rich zircons from the Laoshan I- and A-type granites, Eastern China. *Mineralogical Magazine*, *64*(5), 867–877. https://doi.org/10.1180/002646100549850

Wu, Y. L., Mei, Y. W., Liu, P. C., Cai, C. L., & Lu, Y. L. T. (1987). *Geology of the Xihuashan tungsten ore field*. Geological Publishing House. (in Chinese).

Wunder, B., Meixner, A., Romer, R. L., Feenstra, A., Schettler, G., & Heinrich, W. (2007). Lithium isotope fractionation between Li-bearing staurolite, Li-mica and aqueous fluids: An experimental study. *Chemical Geology*, *238*(3–4), 277–290. https://doi.org/10.1016/j.chemgeo.2006.12.001

Wunder, B., Meixner, A., Romer, R. L., & Heinrich, W. (2006). Temperature-dependent isotopic fractionation of lithium between clinopyroxene and high-pressure hydrous fluids. *Contributions to Mineralogy and Petrology*, *151*(1), 112–120. https://doi.org/10.1007/s00410-005-0049-0

Wunder, B., Meixner, A., Romer, R. L., & Jahn, S. (2011). Li-isotope fractionation between silicates and fluids: Pressure dependence and influence of the bonding environment. *European Journal of Mineralogy*, *23*(3), 333–342. https://doi.org/10.1127/0935-1221/2011/0023-2095

Yang, J. H., Jiantang, P., Junhong, Z., Yazhou, F., Chen, Y., & Yinglong, H. (2012). Petrogenesis of the Xihuashan granite in southern Jiangxi Province, South China: Constraints from zircon U-Pb geochronology, geochemistry and Nd isotopes. *Acta Geologica Sinica-English Edition*, *86*(1), 131–152. https://doi.org/10.1111/j.1755-6724.2012.00617.x

Yang, J.-H., Kang, L. F., Peng, J. T., Zhong, H., Gao, J. F., & Liu, L. (2018). In-situ elemental and isotopic compositions of apatite and zircon from the Shuikoushan and Xihuashan granitic plutons: Implication for Jurassic granitoid-related Cu-Pb-Zn and W mineralization in the Nanling Range, South China. *Ore Geology Reviews*, *93*, 382–403. https://doi.org/10.1016/j.oregeorev.2017.12.023

Zhao, J.-H., & Asimow, P. D. (2014). Neoproterozoic boninite-series rocks in South China: A depleted mantle source modified by sediment-derived melt. *Chemical Geology*, *388*(0), 98–111. https://doi.org/10.1016/j.chemgeo.2014.09.004